Graphenes as Potential Material for Electronics

Jishan Wu, Wojciech Pisula, and Klaus Müllen*

Max-Planck-Institut für Polymerforschung, Ackermannweg 10, D-55128 Mainz, Germany

Received April 4, 2006

Downloaded via UNIV OF COLORADO COLORADO SPRINGS on March 27, 2024 at 20:35:34 (UTC).
See https://pubs.acs.org/sharingguidelines for options on how to legitimately share published articles.

Contents

1. Introduction 718
2. Versatile Syntheses of 2D Graphene Molecules 720
   2.1. Hexa-*peri*-hexabenzocoronenes 720
   2.2. Larger Graphenes 724
   2.3. Chemical Modification of Hexa-*peri*-hexabenzocoronenes 728
3. Thermotropic Behavior of Graphene Molecules in the Bulk 731
4. Alignment of Graphene Molecules in Thin Films and Their Device Applications 734
5. Self-assembly at Solid–Liquid Interfaces 740
6. Novel Carbonaceous Nanostructures by Solid-State Pyrolysis 742
7. Conclusion and Outlook 744
8. Acknowledgments 745
9. References 745

1. Introduction

This article is concerned with well-defined, nanosized polycyclic aromatic hydrocarbons (PAHs) and their uses in organic electronic devices. Although PAHs are generally known to the chemist as key objects of structural organic chemistry, their particular electronic and self-assembling properties also provide opportunities for novel device fabrications.

PAHs can be regarded as two-dimensional graphite segments composed of all-sp^2 carbons and are widely found in the residues of domestic and natural combustion of coal, wood, and other organic materials, and even in interstellar space.[1] They are ubiquitous environmental contaminants and in some cases even carcinogenic.[2] However, there exist only a few examples of analytically pure and functionalized PAHs with high molecular weight. Pioneering contributions to the synthesis and characterization of PAHs were made by R. Scholl and E. Clar in the first half of the 20th century.[1] More recently, the progress of modern synthetic methods and analytical techniques has allowed the efficient synthesis of well-defined PAHs under mild condition.[3] Many theoretical and experimental studies have been performed regarding their geometric, energetic, and magnetic properties.[4] NMR chemical shifts and diamagnetic susceptibilities have served as key experimental criteria when judging the aromaticity of PAHs.[4b] The structural properties of PAHs such as bond orders, bond lengths, and the degree of planarity can be predicted by quantum chemical calculations and compared with spectroscopic and X-ray diffractometric information.[4,5] The thermal and chemical stabilities of PAHs depend not only on their size but also upon the topological arrangement of the benzenoid rings. According to Clar's aromatic sextet rule, PAH molecules can be formulated by circles in a monocyclic system symbolizing the six π-electrons in benzene rings (benzenoid aromatic sextets) and not-fully benzenoid rings that are symbolized in Kekulé style. For a given PAH system, isomer stability increases with the number of sextets.[1b] Thus, *all-benzenoid* polycyclic aromatic hydrocarbons (PBAHs) whose structure can be represented by "full" aromatic sextet rings (i.e., no double bonds) show extremely high stability, high melting points, and low chemical reactivity.

The early discoveries of conducting and semiconducting organic polymers in the 1970s have now led to promising applications in the field of organic electronics.[6] Along these lines, organic chemists have pursued various π-conjugated systems as active components for electronic and optoelectronic devices, such as light-emitting diodes, field-effect transistors (FETs), and solar cells.[7] The key physical processes for these applications are the formation, transport, and recombination of electrical charges. In particular, the mobility of charge carriers in solid-state materials is one of the most important parameters determining device performance.[8] The short-range (local) charge transport can be detected by pulse-radiolysis time-resolved microwave conductivity (PR-TRMC) measurements in which the sample is irradiated by a high-energy electron beam and the local charge carrier mobility deduced from the change of microwave absorption.[9] However, the value of the long-range charge carrier mobility, which can be determined by time-of-flight (TOF) experiments or directly in a field-effect transistor, is usually more important for devices. These electronic mobilities depend not only on the intrinsic electronic properties of the materials but also on the macroscopic order of the molecules in films (*vide infra*).[8d] Therefore, the control of a defined macroscopic state of matter by way of chemical design and physical processing becomes a key issue. In the family of organic materials, higher charge carrier mobilities are typically obtained in organic single crystals; however, poor processability limits their applications.[10] On the other hand, liquid crystalline materials with good solubility have allowed facile solution processing and the fabrication of high-quality thin films.[11] Conjugated polymers and oligomers represent by far the most widely investigated materials for organic electronics.[12] However, the one-dimensional nature of these chain structures constitutes a serious limitation, since it leads to low-dimensional conductors in the solid state.[13,14] Recently, disc-like PAHs as two-dimensional high-purity materials have

* E-mail: muellen@mpip-mainz.mpg.de. Fax: 00 49 6131 379 350. Telephone: 0049 6131 379 150.

10.1021/cr068010r CCC: $65.00 © 2007 American Chemical Society
Published on Web 02/10/2007

Dr. Jishan Wu was born in Hubei province, China, in 1975. He received his B.Sc. degree from Wuhan University in 1997. He then worked on conjugated molecular wires under the supervision of Professor Xianhong Wang and Professor Fosong Wang at the Changchun Institute of Applied Chemistry, Chinese Academy of Sciences, where he obtained a masters degree in polymer sciences in 2000. He performed his doctoral work on the synthesis of new discotic graphitic materials under the supervision of Professor Klaus Müllen at the Max Planck Institute for Polymer Research, and he was awarded his Ph.D. in 2004 from Johannes-Gutenberg University in Mainz. He continued his research on synthesis, characterization, and material application of polycyclic aromatic hydrocarbons in the same group as a project leader. In 2005, he joined Professor J. Fraser Stoddart's research group at the University of California, Los Angeles, where he is currently focused on supramolecular chemistry.

Dr. Wojciech Pisula studied chemical engineering (1996–2001) at the University of Applied Science Osnabrück and at the University of Wales, Swansea, where he gained his Master of Science. During his diploma thesis, he worked on the compatibilization of various blends of immiscible polymers in the group of Professor Jacek Piglowski at the Technical University of Wrocław in the Institute for Organic Technology and Synthetic Materials in collaboration with Professor Claudia Kummerlöwe at the University of Applied Sciences Osnabrück. In 2001, he joined the group of Professor Klaus Müllen at the Max Planck Institute for Polymer Research, where he completed his dissertation in 2005. There, he focused on the control of the supramolecular self-organization of discotic liquid crystalline polycyclic aromatic hydrocarbons with a strong interest in their application in electronic devices. During this time, he worked in the Department of Polymer Physics under the supervision of Professor Tadeusz Pakula. After an additional research year as a postdoctoral scientist in the same group, he has been employed in the Process Technology & Engineering Department at Degussa AG, Hanau.

attracted intensive interest.[15] Typical examples of these materials are triphenylene and hexa-*peri*-hexabenzocoronene (HBC) derivatives. Due to its D_{6h}-symmetry and its large π-systems (three times the size of triphenylene), HBC can be called "super-benzene". Substitution around the aromatic cores by flexible aliphatic chains provides opportunities to control the solubility and thermal behavior, which are

Prof. Dr. rer. nat. Klaus Müllen received his Diplom Chemiker degree (1969) at the University of Cologne after work with Professor Dr. E. Vogel and his Ph.D. degree from the University of Basel, Switzerland (1972), where he undertook research with Professor F. Gersson on EPR spectroscopy. He pursued postdoctoral research at the Swiss Federal Institute of Technology in Zuerich in the group of Professor J. F. M. Oth, where he worked in the field of dynamic NMR spectroscopy and electrochemistry. He received his habilitation there in 1977 and was appointed Privatdozent. In 1979 he became Professor in the Department of Organic Chemistry, University of Cologne, and in 1983, he accepted an offer of a chair in Organic Chemistry at the University of Mainz. He joined the Max-Planck Society in 1989 as one of the directors of the Max-Planck Institute for Polymer Research. His current research interests focus on synthetic macromolecular chemistry, supramolecular chemistry, and materials science.

essential for the processing of these materials. The introduction of aliphatic chains provokes a thermotropic behavior and a discrete phase formation. The side chains increase the disorder and lead to a nanophase separation between the highly ordered aromatic cores, which pack due to π-stacking on top of each other, and the rather disordered alkyl chains that fill the periphery.[16] The resulting superstructure is a columnar organization of disc-shaped molecules, the so-called discotics, which in turn arrange into a two-dimensional array.[17] At elevated temperatures, different phases can be observed that are assigned by the supramolecular order, as characterized by X-ray diffraction,[18] and the molecular dynamics, as measured by solid-state NMR spectroscopy.[19]

The favorable overlap of π-orbitals in adjacent molecules significantly increases the charge carrier mobility. Columnar stabilization by additional interactions, such as hydrogen bonds,[20] decreases the distance[21] between the single building blocks and enhances the charge transport. Values up to 1.1 $cm^2\ V^{-1}\ s^{-1}$ for HBC materials have been detected by the PR-TRMC method.[22] Due to their unique, highly ordered columnar structures and the large π-orbital area of the cores, HBCs are qualified as active semiconductors in organic field-effect transistors and photovoltaic devices. The one-dimensionality of the charge carrier transport along the stacks is ensured by the pronounced intracolumnar packing and the effective filling of the insulating aliphatic chains in between the columns.[23] On the other hand, such specific one-dimensionality is at the same time rather sensitive to structural bifurcation defects.

Hexa-*peri*-hexabenzocoronene (HBC) contains 42 carbons and is a typical example of a PBAH with self-assembly properties.[15b, 15c, 15d] The synthesis optimization of parent HBC has taken a long time since the first synthesis by Clar and co-workers in 1958.[24] Later, Halleux[25] and Schmidt[26] et al. reported alternative methods toward the parent HBC. However, all these synthetic methods yield HBC in low

SAMSUNG EX. 1012 - 2/30

Scheme 1. Clar's Route to HBC

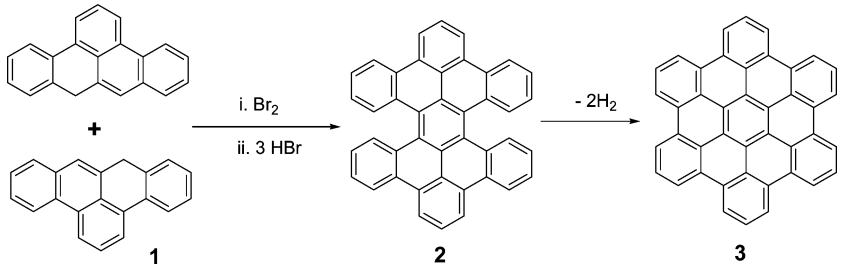

quantities. We have developed an efficient way to prepare HBC by intramolecular oxidative cyclodehydrogenation of hexaphenylbenzene with Cu(II) salts such as $CuCl_2$ and $Cu(OTf)_2$ catalyzed by $AlCl_3$, and this method has later been extended to the synthesis of more complex PAHs with different shapes and sizes.[27]

Related to the formation of thin films, the self-assembly of these disclike molecules in solution and at liquid−solid interfaces is also an important issue. Studies at these interfaces allow predictions of supramolecular order and the electronic properties. The self-assembly behavior of these disclike molecules in solution can be studied by NMR spectroscopy, light scattering (LS), and vapor pressure osmometry (VPO) techniques.[28] Like most conjugated polymers and PAHs, HBC molecules have a strong tendency to aggregate in solution with their association constants dependent on the substituents.[29] The molecular order of thin films resulting after solvent evaporation is related to the size of the aggregates in solution. The interface between organic molecules and substrates is also important because it determines the charge injection and transport in electronic devices.[30] When molecular films of graphenes are immobilized on surfaces, techniques such as scanning tunneling microscopy (STM) have found use. STM techniques not only provide submolecular resolution while visualizing self-assembled monolayers or bilayers but are also suitable for probing the electronic properties of single molecules.[31] Attachment of electron or hole transporting moieties onto the HBC core thus opens the opportunities to fabricate molecular electronic devices.

The highly stable columnar structures of PAHs can further be used as preorganized precursors for the preparation of novel carbon nanostructures at high temperatures. Carbon nanotubes (CNTs) comprise cylindrical graphite layers and have attracted great academic and technological interest because of their unique electronic and mechanical properties.[32] Several methods such as electronic arc-discharge, laser ablation, and chemical vapor deposition (CVD) of small hydrocarbons over metallic nanoparticles (catalyst), are commonly used to prepare CNTs. Since each PAH molecule can be regarded as a graphene segment, we have started to prepare novel carbon micro- and nanostructures from these graphitic discs under mild solid-state pyrolysis reactions. The unique organization of HBCs in the solid state plays an important role for our formation of carbon nanostructures.

In this review article, we will first describe the recent syntheses and structural characterizations of self-organized graphene molecules. Several influencing variables will be discussed including molecular size, shape, and functional substitutions. Second, we will present processing techniques that control molecular order and macroscopic alignment of columnar structures in thin films and their applications in electronic devices. Third, we will focus on STM visualization of graphene self-assembly at the solid−liquid interfaces. And finally, we will describe how novel carbon and carbon−metal nanostructures from disclike molecules can be prepared under solid-state thermolysis process.

2. Versatile Syntheses of 2D Graphene Molecules

2.1. Hexa-*peri*-hexabenzocoronenes

Various methods have been used to prepare well-defined PAHs;[1] among them, Scholl[33] and Kovacic-type[34] reactions using Lewis acid−oxidant combinations as reagents for intramolecular cyclodehydrogenation have been known for a long time. Scholl, Clar, and Zander et al. were the main contributors to the synthesis and structural characterization of various PAHs in the first half of the 20th century.[1] As one important example, D_{6h} symmetric hexa-*peri*-hexabenzocoronene (HBC) and its derivatives have attracted long-term interest due to their high stability, facile self-assembly, and promising applications. The first synthesis of the parent HBC was carried out by Clar and co-workers.[24] They found that the bromination of 2:3−7:8-dibenzo-*peri*-naphthene (**1**) in benzene gave a deep brown precipitate in which three bromine atoms were added (Scheme 1). The precipitate was heated at 153 °C and resulted in the formation of tetrabenzoperopyrene (**2**). Compound **2** was further heated to 481 °C, and HBC (**3**) was obtained as a pale yellow solid, which did not melt even at 700 °C. HBC can also be gained by melting compound **1** with sulfur or by sublimation of the residue from the preparation of dibenzo-*peri*-naphthene. The UV−vis absorption spectrum of the dilute HBC solution in 1,2,4-trichlorobenzene revealed three typical bands named as a low-energy α-band at around 440 nm, a β-band at 360 nm, and a *p*-band at 387 nm, respectively.

Halleux and co-workers later reported the synthesis of parent HBC using two different methods (Scheme 2).[25] The cyclodehydrogenation of hexaphenylbenzene (**4**) by molten $AlCl_3$/NaCl and the reaction of dibenz-1,9;2,3-anthrone (**5**) with $Zn/ZnCl_2$ both produced HBC. Two other hydrocarbons, tetrabenzo-4,5;6,7;11,12;13,14-peropyrene and tetrabenzo-1,2;3,4;8,9;10,11-bisanthene, have been isolated from the reaction of compound **5** with $Zn/ZnCl_2$.

A new synthesis of HBC was reported by Schmidt and co-workers in 1986.[26] As shown in Scheme 3, reaction of the quinone **6** with phenyllithium afforded the diols **7** in 29−46% yield. The diols were cyclized in an $AlCl_3$/NaCl melt (3 min, 120 °C) and then subjected to aromatization with Cu at 400 °C to give HBC (**3**) in 0.4% yield.

All the above synthetic methods involve complicated experimental workup and gave the desired compound in very low yield. Our group has developed an efficient way to prepare HBC and related PAH structures by Scholl-type oxidative cyclodehydrogenation of branched oligophenylenes

SAMSUNG EX. 1012 - 3/30

Scheme 2. Two Different Ways toward HBC by Halleux et al.

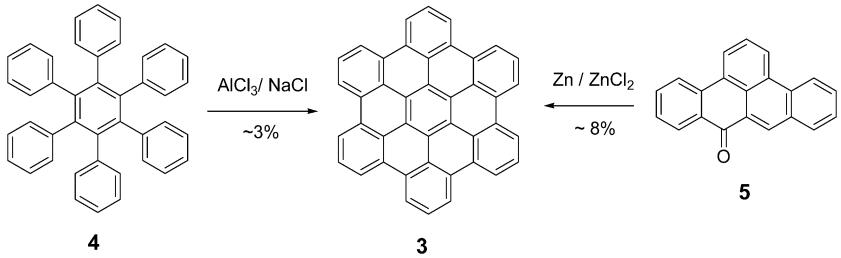

Scheme 3. Synthesis of HBC by Schmidt et al.

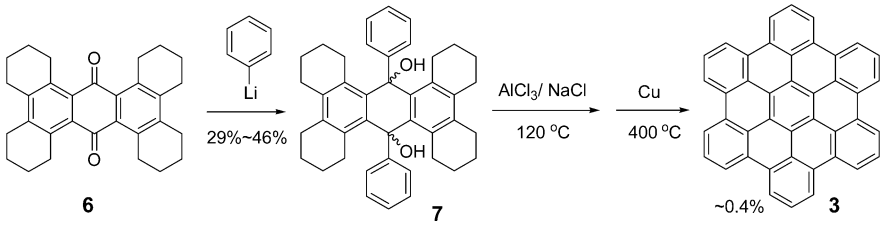

Scheme 4. General Synthetic Route to Sixfold Symmetric HBCs

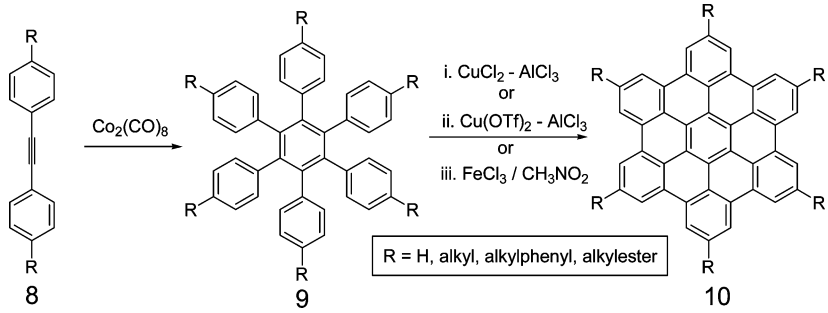

Scheme 5. General Synthetic Route to Lower Symmetric HBCs

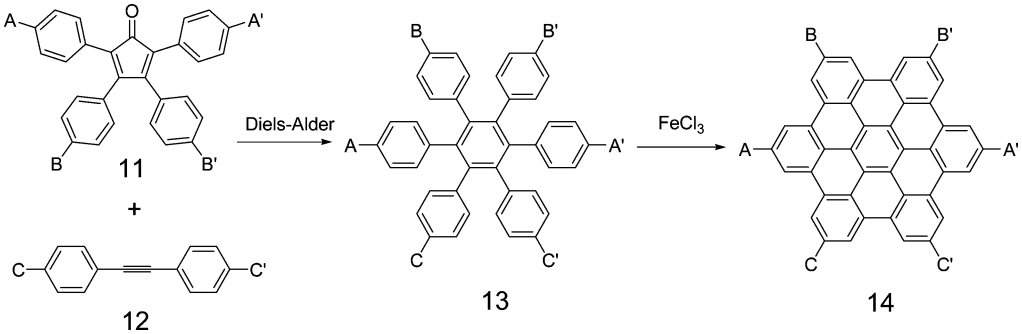

with Cu(II) salts such as $CuCl_2$ and $Cu(OTf)_2$ catalyzed by $AlCl_3$.[27b] Use of the weaker Lewis acid $FeCl_3$ renders the addition of an oxidant unnecessary because $FeCl_3$ possesses an oxidation potential sufficient for the C−C bond formation. The general synthetic protocol is shown in Scheme 4. The hexaphenylbenzenes[35] (**9**) were first synthesized by $Co_2(CO)_8$-catalyzed cyclotrimerization of substituted diphenylacetylenes (**8**), and then cyclodehydrogenation of **9** under different Scholl conditions gave HBC molecules **10** in high yields. Using this method, the parent HBC[36] as well as sixfold symmetric alkyl-,[37] alkylphenyl-,[38] and alkylester-substituted HBCs (**10**) were prepared also in high yield.

HBC derivatives carrying substitutuents in different regioisomeric patterns were synthesized by an alternative route (Scheme 5). Diels−Alder cycloadditions between appropriate tetraphenylcyclopentadienone derivatives (**11**) and substituted diphenylacetylenes (**12**) afforded the hexaphenylbenzene derivatives (**13**), which further underwent oxidative cyclodehydrogenation with $FeCl_3$ to give the fused HBC derivatives **14**.

On the basis of the above synthetic approach, HBCs carrying solubilizing alkyl chains and one or multiple bromo substitutents with different symmetries were synthesized (Figure 1). Subsequent functionalization by transition metal-catalyzed coupling reactions thus afforded HBC derivates with different mesophase properties.[39]

While the synthetic protocol for HBC materials in Scheme 1 is simple, flexible, and high yielding, some limitations have been encountered. First, the synthesis requires multiple steps to occur with hexaphenylbenzene precursors containing the desired functional groups R. Carrying these substituents through several steps can sometimes lead to low atom economy. Second, the identity of R is limited by the tolerance of the cyclotrimerization catalyst (for example, bipyrimidylacetylene can form a complex with $[Co_2(CO)_8]$ and thus cyclotrimerization fails). Finally, the R is limited by its

SAMSUNG EX. 1012 - 4/30

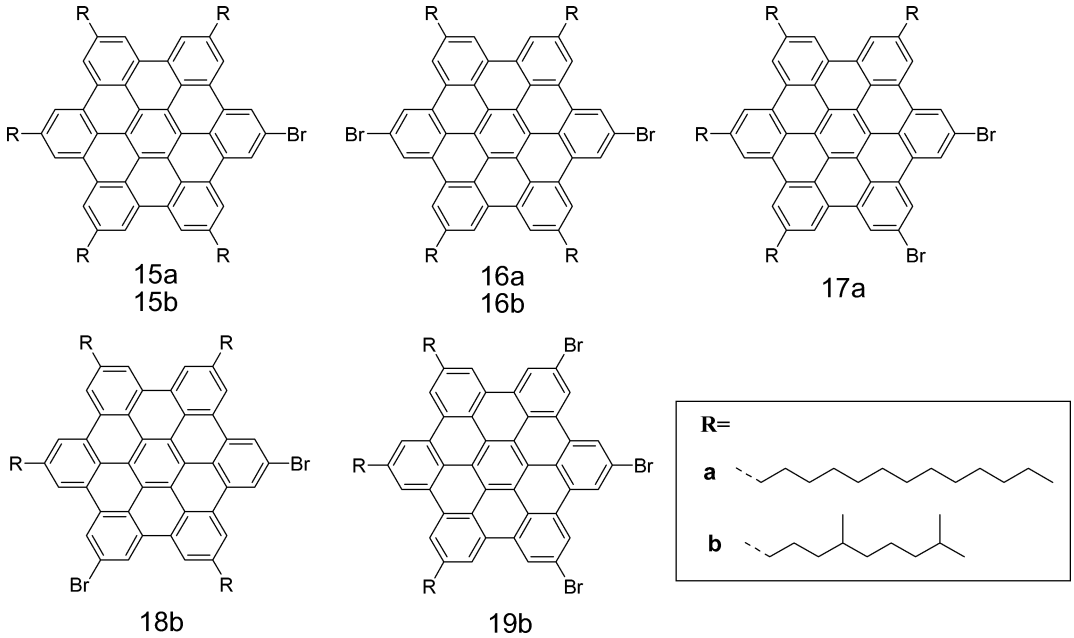

Figure 1. HBC molecules with bromine functional groups.

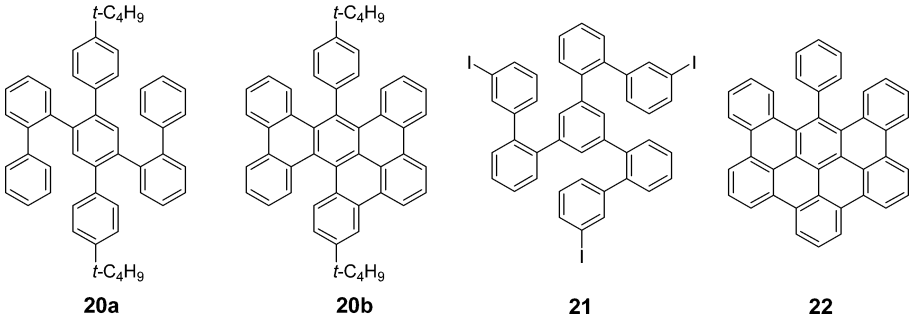

Figure 2. Precursors and intermediate compounds for the synthesis of HBCs.

compatibility with the final oxidation step. For example, cyclodehydrogenation of alkoxy- and alkylthio-substituted hexaphenylbenzenes resulted in ether cleavage.[40] In addition, electroactive moieties such as triaryl amines were excluded, presumably due to the preferential localization of charge on the nitrogen as radical cations.[41] The geometric linkages of the phenyl rings in the precursors also determined the products of the final cyclodehydrogenation reactions. For example, treating 1,4-bis(2-phenylphenyl)-2,5-bis(4-*tert*-butylphenyl)benzene (**20a**) with $FeCl_3$ yielded the partially fused compound **20b** in good yield (Figure 2),[42] while similar oxidative cyclodehydrogenation of precursor 1,3,5-trisbiphenylylbenzene (**21**) worked smoothly and afforded the fully ring-closed HBC molecule in quantitative yield.[43] Little is known about the cyclodehydrogenation; however, a stable intermediate (**22**) has been separated after cyclodehydrogenation of hexaphenylbenzene.[36] This partially ring-closed intermediate suggests a stepwise cyclization mechanism. Theoretical studies have also been conducted to understand these intramolecular Scholl reactions.[44] King et al. predicted that, in the presence of strong protonating reagent, the reaction proceeded in a stepwise arenium cation mechanism instead of a radical cation mechanism.[44a] However, Negri et al. suggested a radical cation mechanism with step-by-step C−C bond formation under the described experimental conditions.[44b] The selectivity of the cyclodehydrogenation of different precursors could be related to the stability and reactivity of the formed radical cations.

To broaden the synthetic scope of HBC materials, several insoluble HBC building blocks carrying active iodine atoms, hexakis(4-iodophenyl)-*peri*-hexabenzocoronene (**23**), hexakis-(4-iodo)-*peri*-hexabenzocoronene (**24**), and a D_{3h} symmetric triiodo HBC disc **25** (Figure 3), were synthesized.[45] Although these building blocks were insoluble in normal solvents, they showed a high reactivity in Pd-catalyzed Hagihara−Sonogashira, Buchwald−Hartwig, and Kumada/Negishi cross-coupling reactions, thus paving a way to a versatile synthesis of functional HBC molecules.[45]

Hagihara−Sonogashira coupling reactions with solubilizing acetylenes worked smoothly with the insoluble iodo precursors and gave a series of soluble extended HBC derivatives **26a−d** and **27a−c** in good yields (Figure 4). The extension of the rigidity in molecule **26a−c** led to highly ordered columnar liquid crystalline phases. For instance, helical stacking of discs in columns was observed in **26b** and **26c** (vide infra).[45b] The electroactive triarylamine-substituted HBCs **26d** and **27b** adopted a coaxial columnar stacking and allowed "double-cable" charge transport along the stacking axis (Figure 4);[43] therefore, they are promising hole transporting materials for organic electronics applications. The amphiphilic, oligoethylene glycol chain-substituted HBC **27c** was soluble in water and methanol.[46] Cylindrical aggregates up to hundreds of nanometers long were detected in water by light scattering measurements. This molecule was therefore used as a template for a sol−gel preparation with porous silica to produce very small pore diameters (∼1

SAMSUNG EX. 1012 - 5/30

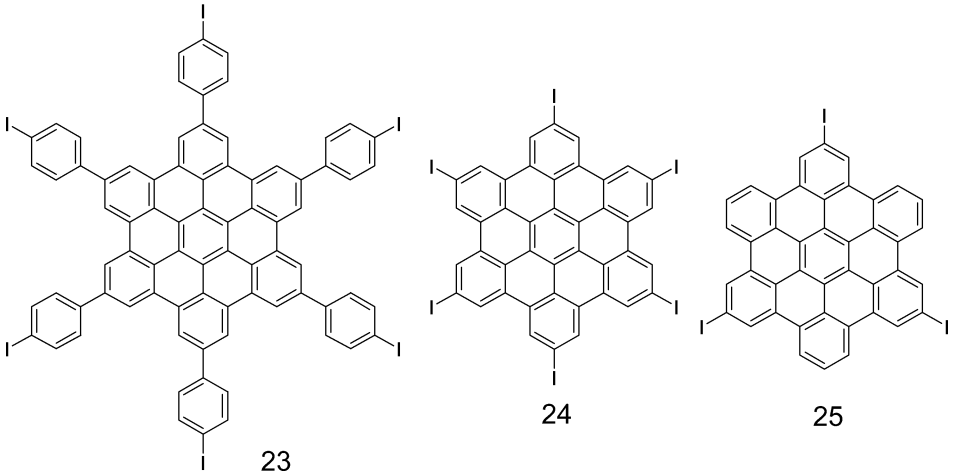

Figure 3. Several insoluble HBC building blocks carrying iodine functional groups.

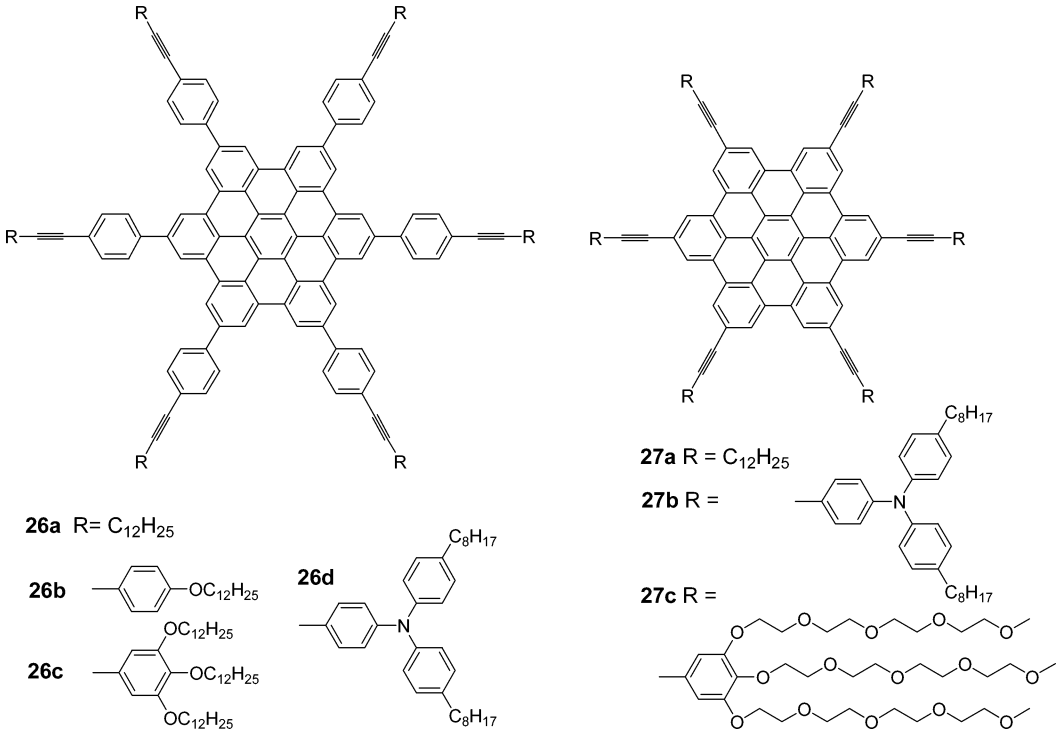

Figure 4. Star-shaped HBC molecules based on molecules **23** and **24**.

nm). Lee et al. have previously reported the synthesis of hexaphenyl and hexabiphenyl hexa-*peri*-hexabenzocorones substituted by branched oligoethylene glycol chains following our synthetic concept (Figure 4).[47] The obtained amphiphilic "hairy discs" formed ordered columnar liquid crystalline phases due to the lateral extension of rigidity from the hydrophobic core as well as strong phase separation tendencies induced by the hydrophilic disordered side chains. These molecules were packed in a face-on arrangement at the water−air interface and on solid surfaces after Langmuir film transfer.

The insoluble HBC building block **25** could also be functionalized by Buchwald coupling reactions and afforded the soluble arylamine-substituted HBC **28** in moderate yield (Figure 5).[43] Similarly, the monoamino- and *para*-diamino-substituted HBCs **29** and **30** were synthesized from the corresponding bromine-substituted HBCs **15a** and **16a**, respectively. Cyclic voltammetry measurements on compound **28** and **30** revealed stepwise oxidation of arylamines yielding mixed-valence compounds, in which obvious intramolecular charge transfer between nitrogen centers through the large HBC π-systems was observed by UV−vis−NIR spectroscopy and electronic spin resonance (ESR) measurements.[43]

Whereas the parent HBC is planar, the permethoxylated HBC **31** is a nonplanar graphene molecule due to the steric congestions between the substituents at the bay positions (Figure 6).[48] The molecule **31** was synthesized according to a similar synthetic strategy as shown in Scheme 4. Single-crystal analysis of molecule **31** revealed that the outer phenyl rings flip up and down in an alternating manner with respect to the inner ring, resulting in a "double-concave" conformation. A significant deviation from the planar geometry, with a maximum angle of $\beta = 17°$, was observed. The nonplanar HBC was a good supramolecular host for fullerene and electron-deficient perfluorobenzene. The analysis of cocystals consisting of compound **31** and fullerene C_{60} revealed that the C_{60} was perfectly included by the complementary double-

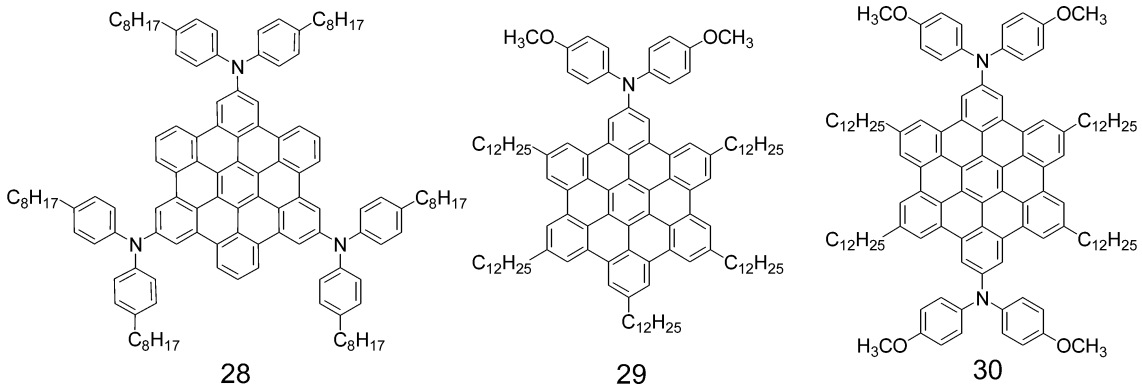

Figure 5. Arylamine-substituted hexa-*peri*-hexabenzocoronenes.

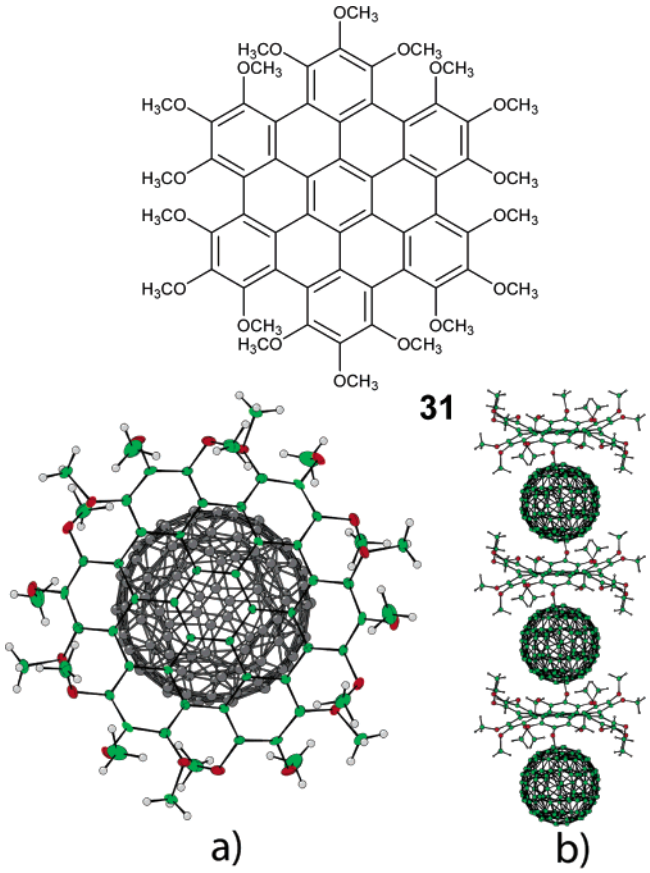

Figure 6. Permethoxylated HBC **31** and its complex with C_{60} fullenrene. (Reprinted with permission from ref 48. Copyright 2005 John Wiley & Sons, Inc.)

concave geometry within a 1D columnar structure (Figure 6). The strong interaction between the C_{60} and the molecule **31** was explained in terms of van der Waals and electrostatic interactions rather than of charge transfer interactions. Molecule **31** also formed a 1:2 complex with hexafluorobenzenes (HFBs); that is, two HFB molecules were accommodated into the cavity formed by the methoxy groups and the interactions were explained as arene−perfluorarene interactions.

As a homonym of hexa-*peri*-hexabenzocoronene, the hexa-*cata*-hexabenzocoronene and its derivatives **32a**−**c** recently have been synthesized (Figure 7).[49] The first synthesis of parent hexa-*cata*-hexabenzocoronene **32a** was reported by Clar et al. in 1965.[50] They prepared the tetraol compound **33** and found that condensation of **33** with copper powder at 400 °C provided the HBC **32a** in about 2% yield after column chromatography. In contrast to the insoluble parent hexa-*peri*-hexabenzocoronene, the hexa-*cata*-hexabenzocoronene **32a** is soluble in normal organic solvents and has a melting point of 516 °C. Recently, Nuckolls et al. reported new syntheses of hexa-*cata*-hexabenzocoronene and its derivatives **32a**−**c** by photocyclization of the bisolefins **34a**−**c** (Figure 7).[49] The yields of the final steps are usually more than 80%, therefore allowing large-scale preparation of HBC. As disclosed by single-crystal analysis, due to the steric congestion in its proximal carbon atoms, the aromatic core was distorted away from planarity and the three intersecting pentacene subunits contorted into a zigzag conformation. After the attachment of flexible alkyl chains, the nonplanar compound **32c** formed an ordered columnar liquid crystalline phase.

2.2. Larger Graphenes

The $FeCl_3$- or $Cu(OTf)_2$−$AlCl_3$-mediated oxidative cyclodehydrogenation of branched hexaphenylbenzene derivatives was also applied to the synthesis of giant graphene molecules with different sizes and shapes. Increasing the size of the core of discotic materials is predicted to improve the order of columnar superstructures due to the large overlaps of π-surfaces and thus enhance their charge carrier mobility.[51] We have accordingly investigated the synthesis of parent and alkyl-chain-substituted discotic PBAHs with cores significantly larger than HBC (Schemes 4 and 5). Appropriate branched oligophenylenes were first prepared by Diels−Alder reactions and then subjected to oxidative cyclodehydrogenation to give planar graphene discs. In this way, graphene molecules containing 90 (**35**),[52] 96 (**36a**−**f**),[53] 132 (**37**),[54] 150 (**38**),[52] and 222 (**39**)[55] carbon atoms in their cores and different substituents became available (Figure 8). The synthesis of larger graphene discs, in which $FeCl_3$ or $Cu(OTf)_2$−$AlCl_3$ was applied as the reagent, required a large excess of oxidant and longer reaction times. We have described that the dodecyl- (**36a**), phytyl- (**36b**), and carbomethoxyphenyl- (**36e**) substituted super-phenalenes were readily soluble in normal organic solvents. In contrast, superphenalenes with more solublizing 4-dodecylphenyl (**36d**) or 3,7-dimethyloctyl (**36c**) chains showed very poor solubility.

While this result was somewhat surprising, a careful investigation using MALDI-TOF mass spectroscopy with different matrixes has suggested that the good solubility of compound **36a** (**C96**−**C12**) could be induced by the presence of partially fused intermediate compounds. However, it has to be emphasized that MALDI-TOF spectrometry cannot be used for the determination of the relative quantity of the impurities in the sample. The best way to gain such data is

SAMSUNG EX. 1012 - 7/30

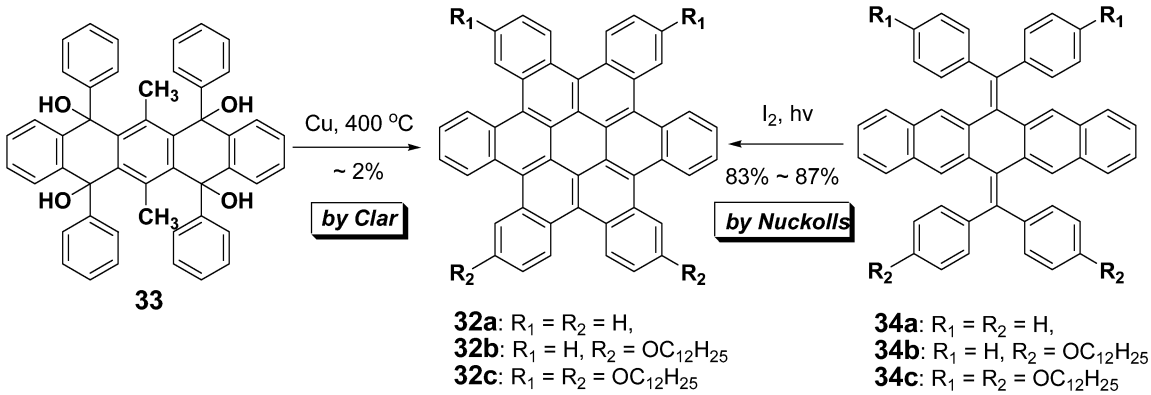

Figure 7. Hexa-*cata*-hexabenzocoronene and its derivatives synthesized by Clar and Nuckolls et al.

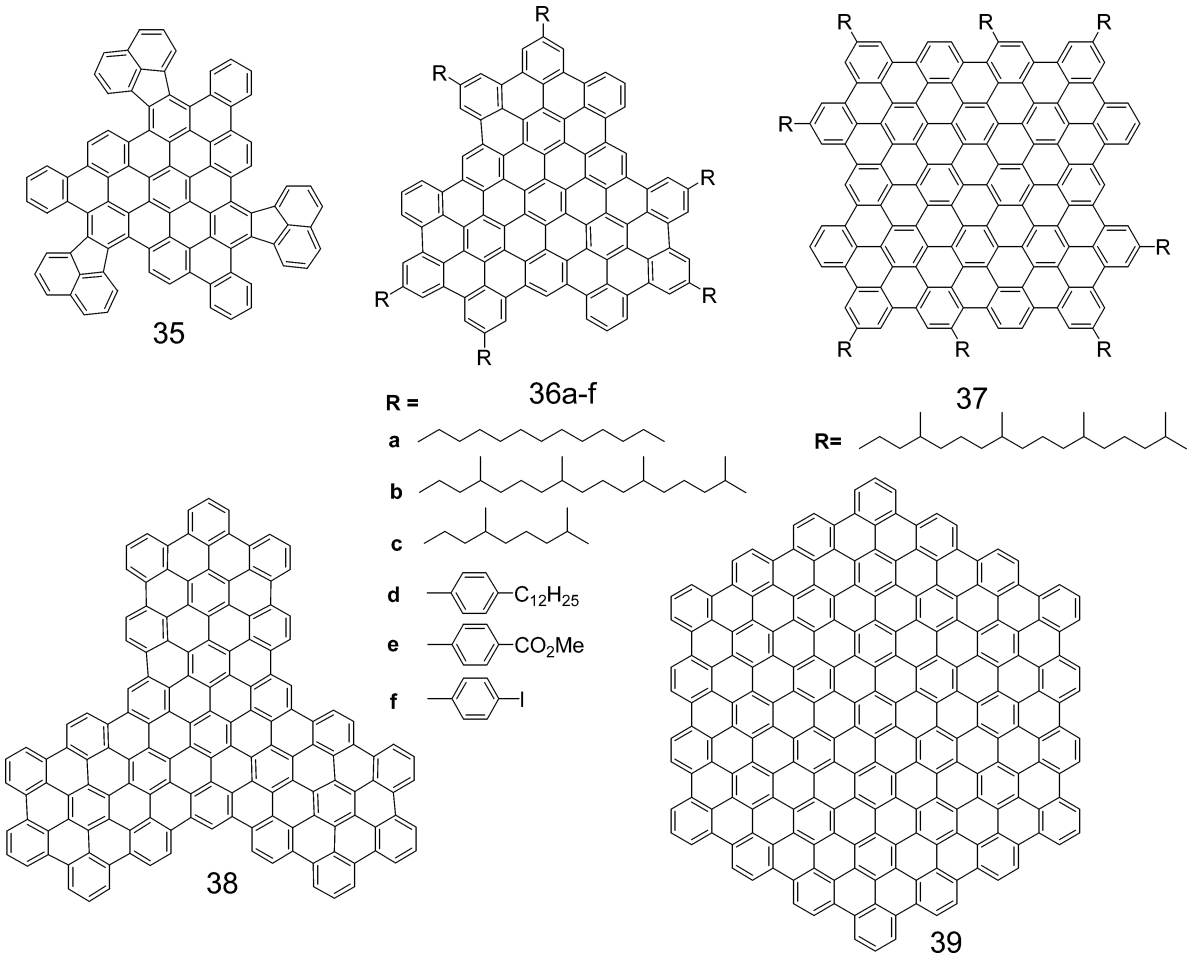

Figure 8. Large graphene molecules with different symmetries.

the recording of solution NMR spectra, which did not succeed so far for **36a** due to the aggregation propensity of the molecules in solution.

A complete cyclodehydrogenation of large oligophenylene precursors needs careful control of the experimental conditions (e.g., time, oxidants, and the amount of reagent), and the products should be determined by combined methods. The insoluble 4-iodophenyl-substituted super-phenalene **36f** was also synthesized and, like its HBC counterpart **23**, could be functionalized by Pd-catalyzed Hagihara−Sonogashira coupling reactions even when the product was also virtually insoluble.

The C150 disc (**38**) was prepared from compound **21** and is the largest disc with threefold symmetry yet made.[52] The C90 disc (**35**) was nonplanar, based on molecular model calculations, due to the five-membered rings and therefore offered a possibility to subsequently make bowl-shaped molecules by flash vacuum pyrolysis.[52,56] Both compounds were characterized by MALDI-TOF mass spectroscopy, solid-state UV−vis absorption, and Raman spectroscopy. For the D_{2h} symmetric graphene disc C132 (**37**), the long flexible phytyl chains were required to impart enough solubility in the normal organic solvents. Giant graphite disc **39** is the largest polycyclic hydrocarbon structure characterized to date.[55] The insoluble product was characterized by isotope-resolved MALDI-TOF mass spectroscopy as well as solid-state NMR spectroscopy. The solid-state UV−vis absorption spectrum revealed a broad long-wavelength absorption band in the UV−vis region from 250 to 1400 nm, indicating an extended conjugation and strong π-stacking between the giant discs.

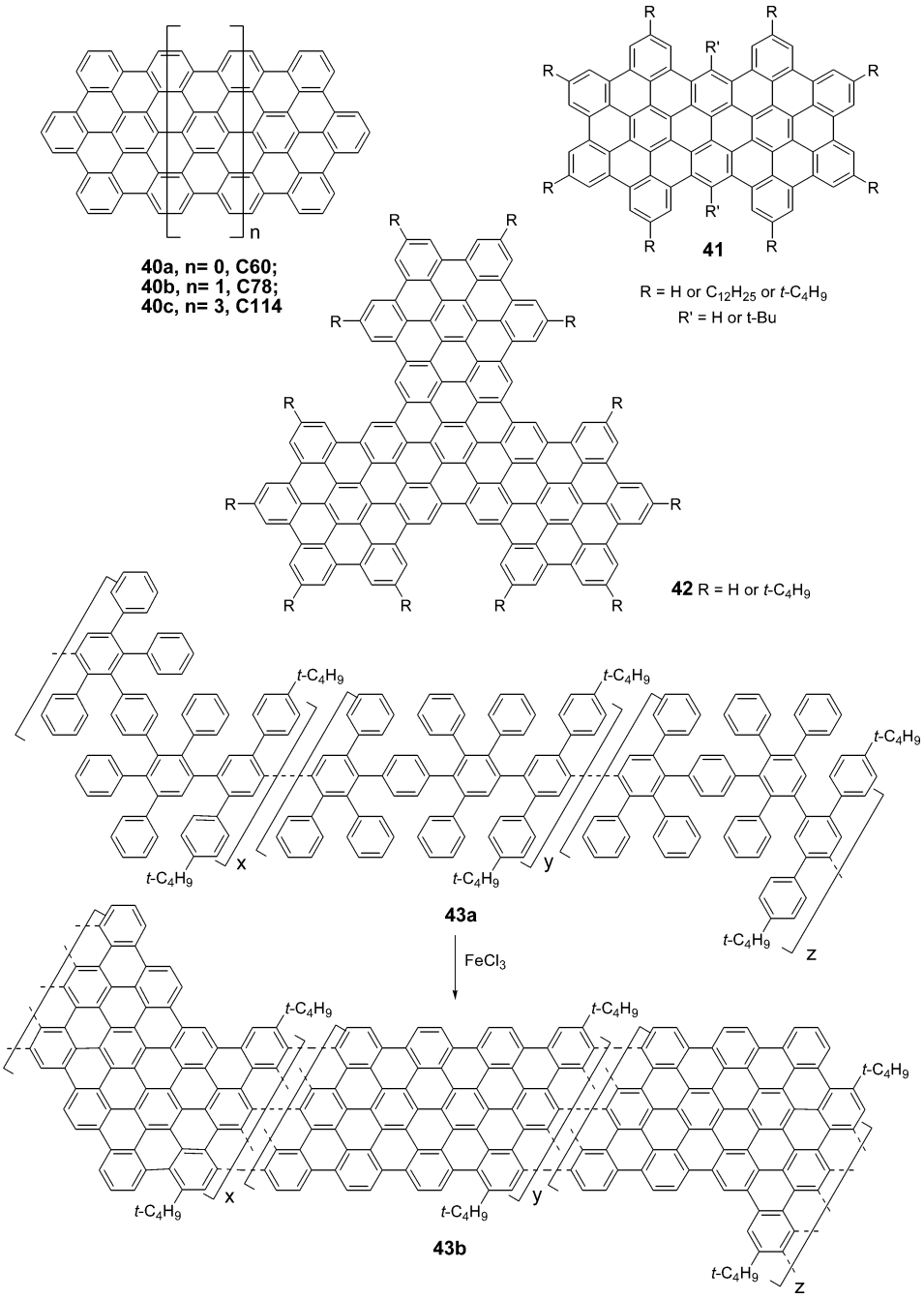

Figure 9. One-dimensional extend graphite ribbons.

The optical absorption properties of graphitic discs with different sizes were studied, and it was found that the maximum wavelength of the lowest energy absorption band (α-band) increased linearly and broadened with the number of "full" six-membered rings.[15b] This behavior is very similar to that of linear conjugated oligomers in which the absorption maximum red-shifts with increased chain length below the effective conjugation length.[14] The concept of completely planarizing large oligophenylenes reaches its limit when the branched oligophenylene becomes so large that the oxidative cyclodehydrogenation can only partially take place. For example, planarization of a C474 oligophenylene dendrimer yielded a partially closed three-dimensional (3D) graphite propeller.[57] Exact structural characterizations were extremely difficult given the insolubility of giant graphite segments. The novel 2D and 3D graphite structures showed a pronounced "charge storage" capacity upon alkali metal reduction and thus have potential applications in lithium storage (vide infra).[58]

While further 2D extension became more and more demanding, extension at one dimension yields ribbon-like graphene structures. A series of well-defined graphite ribbons **40a**−**c** containing 60, 78, and 114 carbon atoms at the core were prepared by a similar concept via a multistep procedure (Figure 9).[59] In analogy to the case of effective conjugation lengths in conjugated polymers, the electronic absorption maximum red-shifted with increasing molecular aspect ratio due to the ever-increasing delocalized π-surface. Two "superacenes" (**41** and **42**) in which two or three HBCs are annealed, as in their structural analogues "naphthalene" and "triphenylene", were also prepared.[60] Attachment of flexible alkyl chains onto the core leads to formation of an ordered columnar liquid crystalline phase.

SAMSUNG EX. 1012 - 9/30

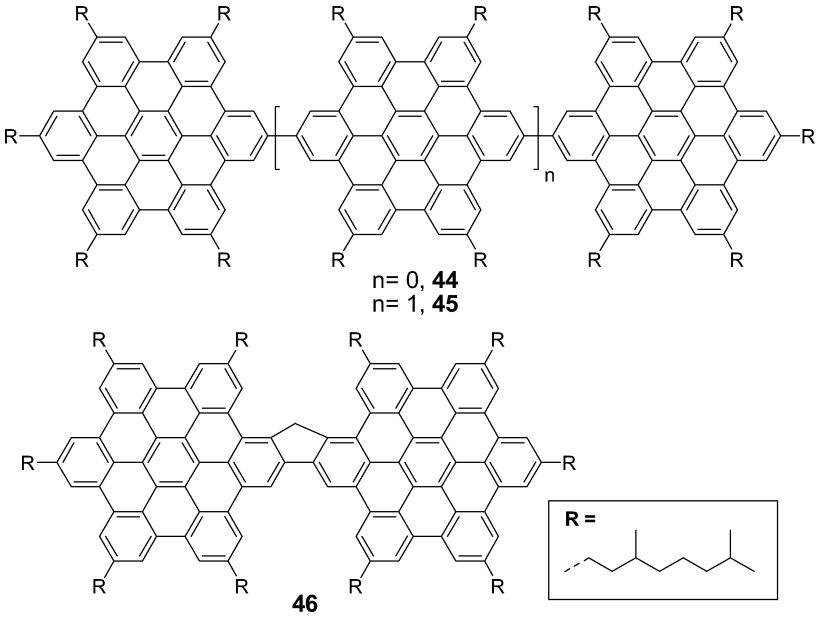

Figure 10. Oligomers of hexa-*peri*-hexabenzocoronenes.

A derivative of **41** carrying two *tert*-butyl substituents was prepared by a novel approach, and it showed extraordinarily high solubility and an effective suppression of aggregation. This was due to a distortion of the aromatic core by bulky *tert*-butyl groups located in the indentation of the aromatic rim in combination with the solubilizing effects of alkyl chains in the corona. Therefore, not only did the processing and purification of the materials with standard laboratory techniques become possible, but also this was the first example of recording of structure-rich UV−vis and a resolved ^{1}H NMR spectra for an aromatic system two times larger than hexa-*peri*-hexabenzocoronene. The structural investigation by X-ray scattering showed a columnar self-assembly of the molecules. By removing the *tert*-butyl groups, the fully planar system **41** was gained, which suffered from the same analytical restrictions as the compounds prepared *via* the oligophenylene route (**36**). The aromatic signals in the ^{1}H NMR spectra could not be resolved anymore even at high temperatures, and the UV−vis spectra lost the detailed band structure. The solubility properties, however, differed severely. While the compounds prepared by the oligophenylene route showed a good solubility in standard organic solvents, the other material was highly insoluble. This indicated that the presence of partially fused intermediates exerts a distinct influence upon the solution behavior, although no clear quantification of the side products could be achieved.

One-dimensional polymeric graphite ribbons (**43b**) were synthesized by intramolecular oxidative cyclodehydrogenation of soluble branched polyphenylenes **43a**.[42a] While the insolubility of the resulting graphite ribbons **43b** precluded standard spectroscopic structure elucidation, their electronic and vibrational properties were probed by solid-state UV−vis, Raman, and infrared spectroscopy and their morphology was studied by high-resolution transmission electron microscopy (HRTEM). A wide and unstructured absorption band covering the visible range of the electronic spectrum ($\lambda_{max} \sim 800$ nm) was observed, confirming the highly extended conjugated framework. The profile of the visible Raman spectrum of the material was characterized by two strong bands (at 1603 and 1322 cm^{-1}), corresponding to the G and D bands of graphite. TEM images of **43b** disclosed two different domains: one contains an ordered graphite layer structure with a layer distance of ca. 3.8 Å, while the other appears as a disordered area. The lack of order in the latter may be explained by the nonlinear structure of the obtained graphite ribbons and the random stacking of the molecules during the precipitation.

Linearly connected HBC oligomers, and their corresponding polymers, have also been synthesized (Figure 10).[61] The UV−vis and fluorescence spectra of HBC dimer **44**, trimer **45**, and the corresponding polymer are very similar to those of the individual HBC units, indicating a weak electronic coupling between the subunits. This can be explained by large angles of torsion between the HBC units and the small atomic orbital coefficients of the bridgehead carbons. By contrast, the methylene bridge in **46** induces copolanarity of the two HBC units, which improves the π-conjugation and suppresses the geometrical relaxation of the backbone upon electronic excitation. These effects lead to a more prominent 0−0 transition band in the fluorescence spectrum than is seen for HBCs. Ordered columnar stacking was detected by X-ray diffraction measurements for compounds **44**−**46** but not for *ortho*-connected HBC trimers in which large torsion between the HBC units suppresses the columnar aggregation.

The nature of the PAH periphery plays an important role in their electronic properties and chemical reactivity. According to Clar's aromatic sextet rule, all-benzenoid graphitic molecules with either "armchair" and/or "cove" peripheries normally show extremely high stability.[1b] However, the PAHs with "acene-like" and "quinoidal" peripheries have higher energies and thus show higher chemical reactivity.[62] Several all-benzenoid hydrocarbons **47**−**50** with "cove"-type instead of "armchair" peripheries have been prepared (Figure 11) according to a similar synthetic concept.[36,63] The resonances of the protons in the "cove" position were strongly shifted to low-field in ^{1}H NMR spectra due to the deshielding of the aromatic surroundings. It is known that the UV−vis and fluorescence peaks of the "acene" series undergo a dramatic red-shift when the number of six-membered rings increases from naphthalene to hexacene.[64] In contrast, the shifts for all-benzenoid PAHs with either "cove" or "armchair"-type edges were small.

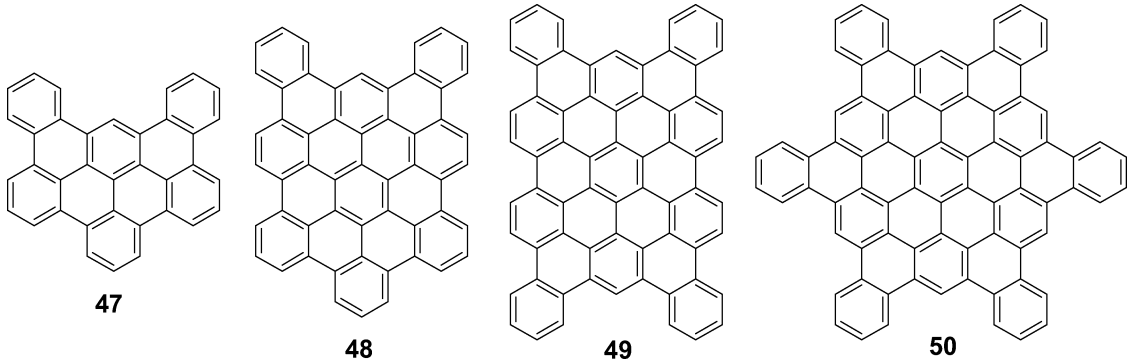

Figure 11. Several all-benzenoid hydrocarbons with "cove"-type peripheries.

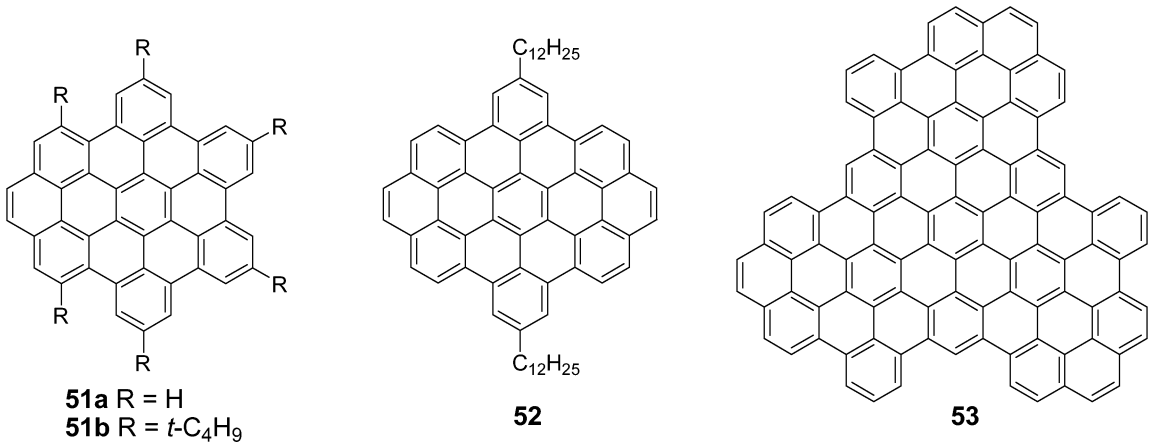

Figure 12. Graphene molecules with partial "zigzag" peripheries.

Graphitic molecules with partial "zigzag" peripheries such as **51a**,**b**, **52**, and **53** (Figure 12) were synthesized[65] and revealed that the addition of two, four, or six extra π-centers onto the all-benzenoid graphitic molecules influences their electronic properties, chemical reactivity, and two- and three-dimensional self-assembly. The absorption maximum of **51a** (λ_{max} = 380 nm) showed a bathochromic shift with respect to the corresponding band of HBC **3** (λ_{max} = 359 nm). Reducing the symmetry increased the intensity of the $0 \rightarrow 0$ band of the α (or L_b) transition (486 nm) in the fluorescence spectrum of **51a**, which is otherwise very weak (symmetry forbidden) for the D_{6h} symmetric unsubstituted HBC. Single-crystal analysis of **51b** disclosed that the molecule is bent because of the steric interactions between *tert*-butyl groups. This nonplanarity also hindered the formation of columnar assemblies.[65a] The graphitic molecules **52** and **53** with more extended "zigzag" character also showed a bathochromic shift with respect to their parent PAH without "zigzag" edges.[65] The additional two, four, or six π-centers also provided reactive sites for further functionalization, e.g., preparation of its corresponding K-region oxide, thus opening up a wide range of "graphene" chemistry.

Similar to the conjugated macrocycles or discs,[28] the alkyl- or alkylphenyl-substituted HBCs tended to aggregate in solution due to the strong π-stacking of the discs. This has been studied by concentration and temperature-dependent NMR measurements assisted by nonlinear least-squares analysis of the experimental data.[66]

2.3. Chemical Modification of Hexa-*peri*-hexabenzocoronenes

The aggregation of the discs has a great influence not only on their order in thin films but also on their photophysical and electronic properties.[67] To further control the self-assembly of HBCs in solution, bulky substituents such as rigid oligophenylene dendrons were attached onto the HBC core by Diels−Alder cycloaddition reactions from the ethynylene-containing HBCs such as **26a** (Figure 13).[45b] The rigid dendrons in molecule **54a** suppressed the $\pi-\pi$ stacking of the HBC cores to a certain extent, and a slow monomer−dimer equilibrium was observed on the NMR time scale.[66] This unique equilibrium could be controlled by temperature, concentration, and solvent, and it afforded discrete monomeric or dimeric species. Further structural modifications, such as the replacement of dodecyl groups in **54a** with hydrogen atoms, resulted in the stable dimer structure **54b** due to diminished steric hindrance (Figure 13). The experimental data was supported by quantum chemical calculations. Attachment of the dendron arms more closely to the HBC core resulted in molecule **55**, which existed only as a nonaggregated monomer (Figure 13). UV−vis absorption and fluorescence spectra of these discrete species revealed obvious differences in their electronic and optoelectronic properties that can be explained by the existence or absence of π-stacking interactions. Functional moieties such as electron acceptor perylene monoimide (PMI) were also introduced at the peripheries of the dendrons by Diels−Alder reactions between compound **26a** and PMI-substituted tetraphenylcyclopentadienones, which resulted in HBC−PMI dyads **54c**. This molecule served as a model compound to understand the energy and electron transfer between the HBC donor and the PMI acceptors. Efficient intramolecular energy transfer from the excited HBC core to PMI moieties was detected.[68]

The inclusion of heteroatoms, such as nitrogen, into the graphene molecules not only changed their electronic properties but also offered the possibility of making novel PAH-

SAMSUNG EX. 1012 - 11/30

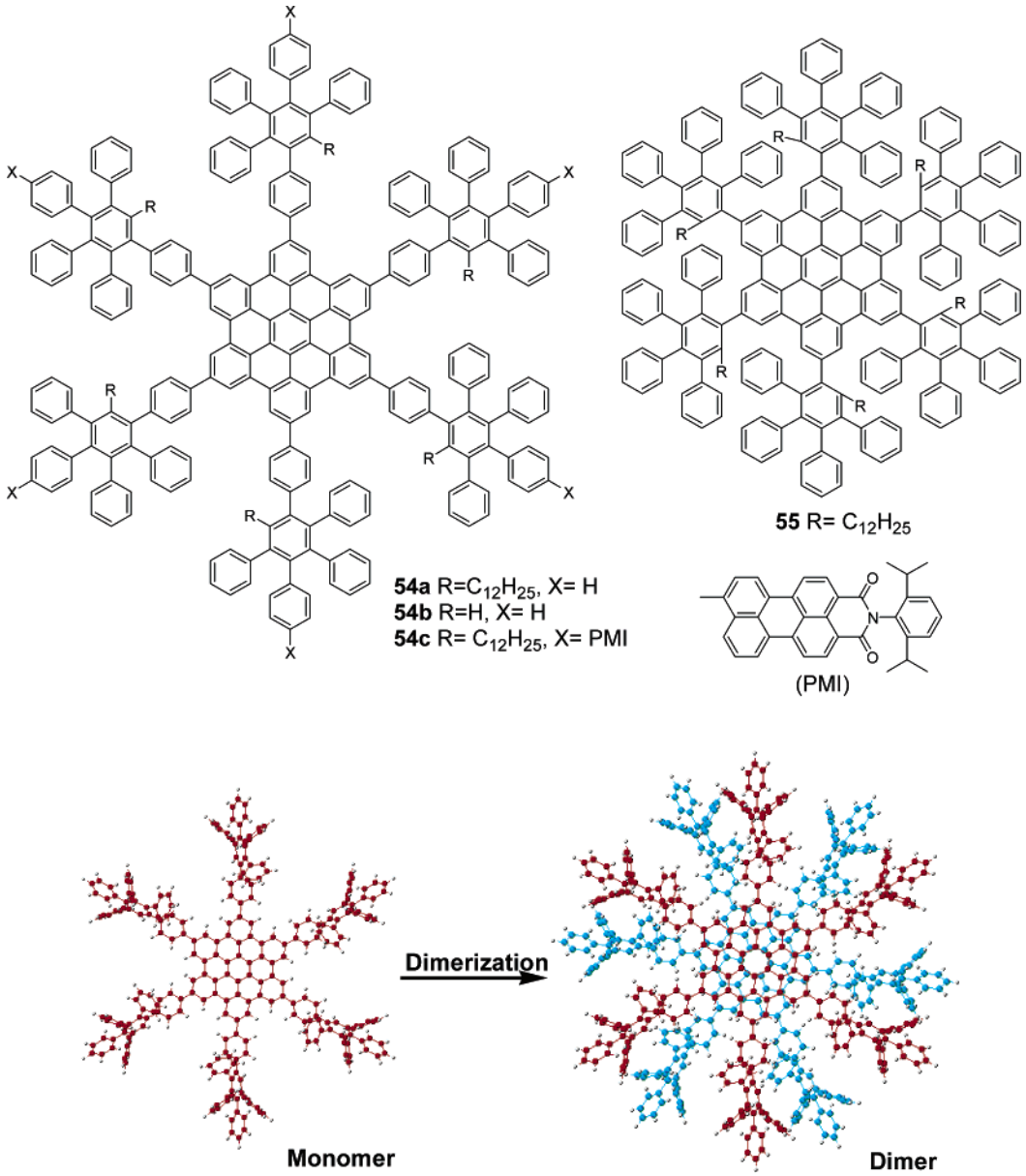

Figure 13. Dendronized HBC molecules and their unique self-assembly in solution. (Reprinted with permission from ref 66. Copyright 2004 American Chemical Society.)

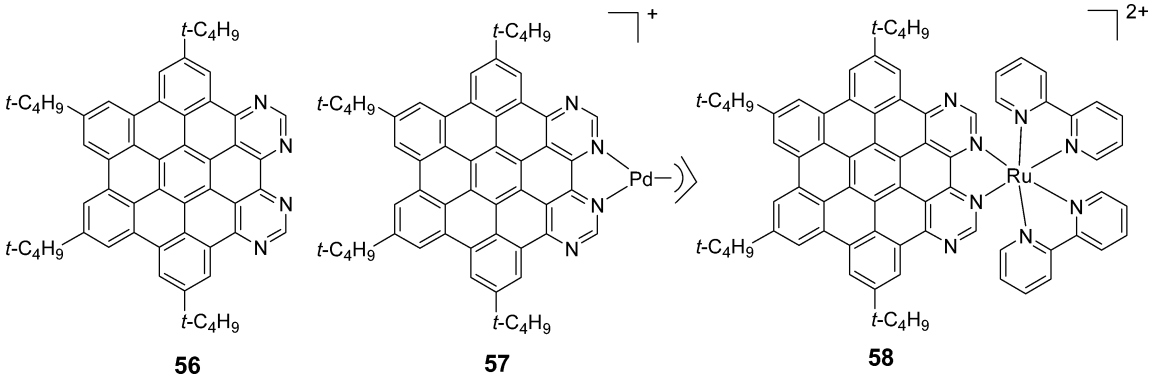

Figure 14. Nitrogen-containing HBC and its metal complexes.

based organometallic complexes. Draper and co-workers first reported a four-nitrogen-containing "super-benzene" molecule **56** which was synthesized by a similar process to those of low-symmetry HBCs (Figure 14).[69] The presence of N atoms increased its overall electron-accepting properties by comparison to the all-C analogue, and addition of acid quenched the green emission. Later, the authors reported complex formation of this graphene ligand with Pd(II) and Ru(II) metal salts.[70] As a result of complexation, the strong green emission of **56** was quenched in the complexes **57** and **58**. The Pd(II) coordination in complex **57** caused a red-shift in the low-energy absorptions and a decrease in the

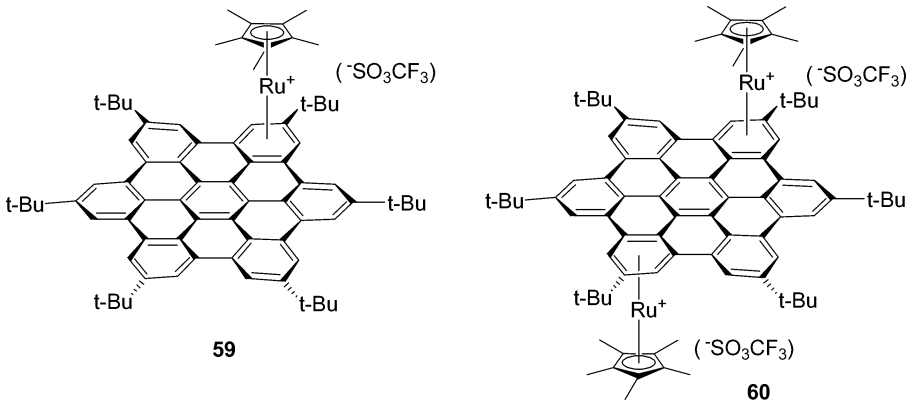

Figure 15. HBC−Ru complexes.

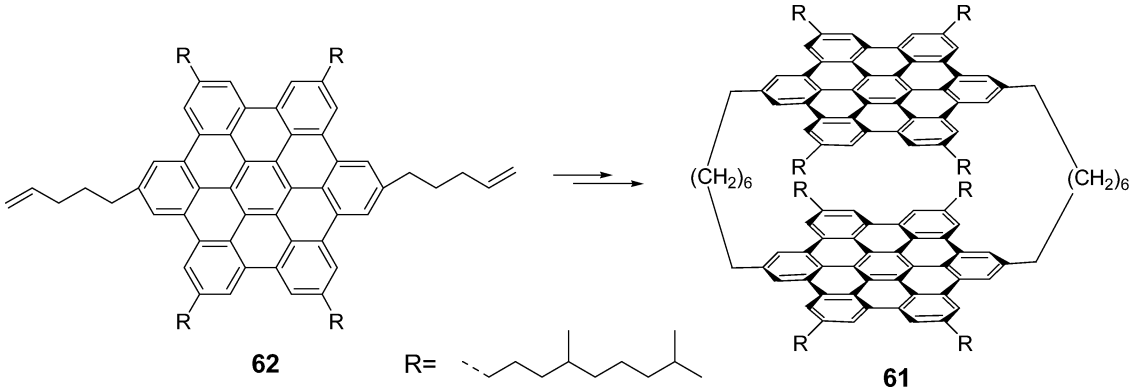

Figure 16. Synthesis of a HBC cyclophane.

intensity of the n−π* absorptions. The Ru(II) coordination complex **58** was a "black" metal−ligand charge transfer (MLCT) absorber and a near-IR emitter, and it has potential applications in solid-state electroluminescence devices.

Transition-metal complexes of polycyclic aromatic hydrocarbons with PAHs used as arene ligands have attracted intensive interest in current organometallic chemistry.[71] Two η^6 transition-metal complexes of HBC derivatives, compounds **59** and **60** (Figure 15), were prepared by the reactions of $[Cp^*Ru(NCMe)_3]^+$ with hexa-*tert*-butyl-*peri*-hexabenzocoronene in refluxing CH_2Cl_2.[72] Single crystal analysis revealed that in both molecules the Ru atom loaded on the top of the outside phenyl ring instead of the inner phenyl ring. In the bis-Ru-HBC complex (**59**), the two Ru atoms were located on the *para*-connected benzene rings and adopted an *anti*-arrangement at opposite sides of the HBC plane. Obvious electronic communication between the two Ru(II) centers was determined by cyclic voltammetry, where two reduction waves for Ru(II) were observed.

Cyclophanes constitute an important molecular framework that organic chemists have been pursuing for a long period of time.[73] Cyclophane **61**, with the largest-to-date aromatic hydrocarbon (HBC), was prepared (Figure 16) using an intermolecular ring-closing olefin metathesis of diene HBC **62**.[74] The metathesis reaction was performed in a 0.4 mM toluene solution with Grubbs catalyst ($[(PCy_3)_2Cl_2Ru{=}CHPh]$), and the good yield arose from the template effect induced by the π-stacking of the HBCs in solution. The olefin linkages were then quantitatively hydrogenated over Pd/C to produce the flexible alkyl chains-linked cyclophane **61**. Solution ^{1}H NMR spectroscopic studies of these cyclophanes indicated a face-to-face intramolecular arrangement of the discs with a slight lateral displacement at room temperature. The covalent linkages did not cause a measurable variation in the inter- and intramolecular stacking, and well-defined columnar liquid crystalline phases similar to the arrangement of monomeric discs were detected in the bulk state.[74] Self-assembly into two-dimensional crystals at a solid−liquid interface was visualized by STM, and the electronic properties of single molecules were assessed by scanning tunneling spectroscopy and revealed an unsymmetric diode-like behavior.

Catalytic hydrogenation of aromatic hydrocarbons has been found to be unpredictable and uncontrollable in many cases.[75] The hydrogenation of parent and alkylated HBC **10** was investigated, and highly regiospecific hydrogenated products, such as the peralkylated coronene derivatives **63**, were obtained (Figure 17).[76] The HBC derivatives were thereby combined with Pd/C (10 wt %) in dry THF, pressurized to 55−65 bar of H_2, and heated to 60 °C. The hydrogenation of *n*-alkyl chain-substituted HBCs provided the peralkylated coronenes **63** in nearly quantitative yield. The parent HBC, however, gave a lower yield (10%) even after a long reaction time, most probably due to its poor solubility. The puckered-ring periphery of these new discs did not prohibit self-assembly to columnar structures in a fashion similar to that of planar HBC precursors but decreased the isotropic temperature by ∼300 °C relative to the latter. The charge carrier mobility and lifetime within the bulk materials were in the same range as those previously found for HBCs. A similar conversion of a homologue with 60 core carbons (**41a**) to the first peralkylated circumbiphenyl **64** was also achieved.[54]

The "Janus" molecular architecture, where one face of the molecule is incompatible with the other, is known for copolymers,[77] rigid conjugated polymers with amphiphilic side chains,[78] and recently, well-defined amphiphilic conjugated π-systems.[79] These materials are interesting due to their

SAMSUNG EX. 1012 - 13/30

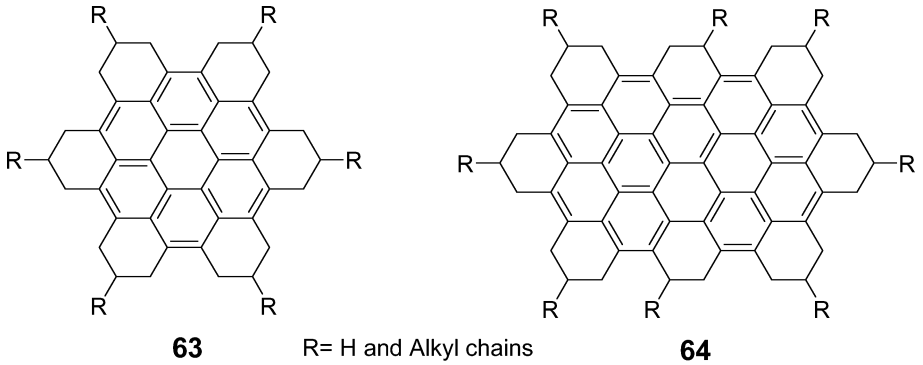

Figure 17. Regiospecific hydrogenation product of graphene discs.

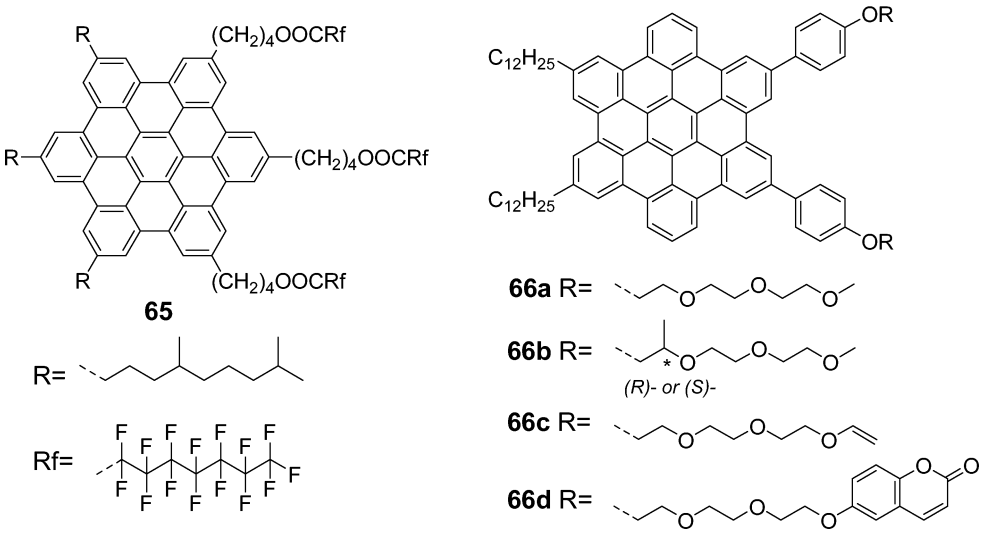

Figure 18. "Janus"-type amphiphilic HBCs.

new properties (in the bulk, at the interface, and in the solution) induced by phase separation of their faces. "Janus"-type HBCs such as **65** and **66** were thus prepared (Figure 18). The alkyl- and fluorinated alkyl chains-substituted HBCs **65** were made starting from tribromo-HBC **19b**.[80] The mixing and demixing controlled the hierarchy of the organizing forces leading to a lamella superstructure as a function of temperature. Recently, Aida's group reported that a gemini-shaped hexa-*peri*-hexabenzocoronene amphiphile **66a** (Figure 18), bearing two paraffinic long alkyl chains on one side and two triethylene glycol (TEG) chains on the other, self-assembled into graphitic nanotubes.[81] Physical stabilization of these self-assembled nanotubes was achieved by attachment of cross-linkable allylic functionalities at the termini of the TEG chains, followed by acyclic diene metathesis reaction (**66c**).[81c] Although compound **66c** is highly soluble in halogenated solvents and no tubular assemblies were formed upon slow evaporation, cross-linking by metathesis in CH_2Cl_2 resulted in the spontaneous formation of covalently stabilized graphitic nanotubes. Later, the authors reported that the coumarin-appended HBC amphiphile **66d** also self-assembled into similar graphitic nanotubes, and the tubular structures could be stabilized by photodimerization of the coumarin pendants at solid state to give insoluble materials.[81d] On the other hand, the cyclobutane derivatives formed upon photodimerization can undergo photochemical cleavage upon irradiation of UV light to give soluble compounds. By taking advantage of this reversible solubility change, they developed both negative and positive patterns of the nanotubes by a lithographic postprocessing.

Stabilization of columnar superstructures formed in discotic liquid crystals is important for optical and electrical applications (vide infra). HBC derivatives form highly ordered columnar mesophases, and such phases can be stabilized by *in situ* polymerization of the HBC monomers, for examples, the acryloyl or methacryloyl groups-substituted HBCs **67a**−**b** and the trifluoroethene-substituted HBC **68** (Figure 19). The former underwent a thermal polymerization to give a cross-linked HBC network in which the columnar superstructures were preserved.[82] The HBC monomer **68** was also able to undergo a thermal polymerization and copolymerization to perfluorocyclobutyl networks containing HBC columns.[83]

In summary, graphene molecules with different sizes, shapes, and functionalities have been prepared by modern organic synthetic methods. This can be achieved through fine molecular design, where the rich chemistry of the graphene molecules offers the opportunity to effectively tune their thermal behavior, solubility, and intrinsic order in the bulk state. These items open the opportunity for the creation of a defined macroscopic state of matter of the material by processing from the melt or from solution.

3. Thermotropic Behavior of Graphene Molecules in the Bulk

The attachment of flexible aliphatic chains to the PAH's periphery, as depicted in section 2.1, is an elegant tool to introduce processibility of these materials. The wide variety of types and geometries of the substituents allows fine-tuning of the solubility and isotropization temperature, which are

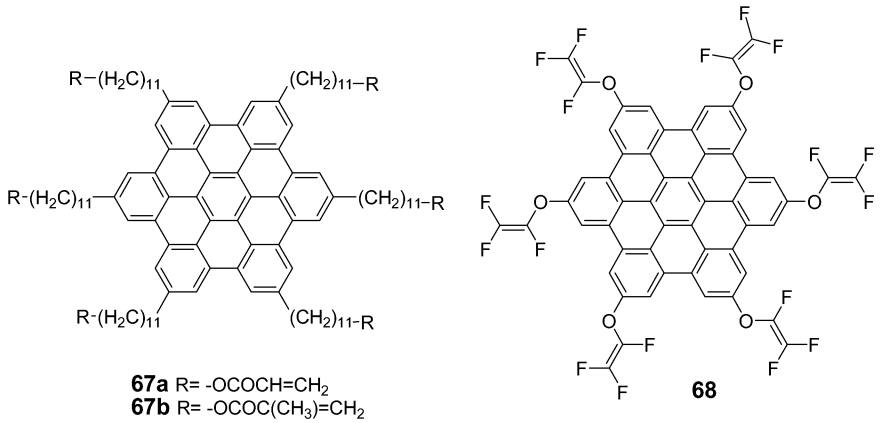

Figure 19. HBCs carrying cross-linkable functional groups.

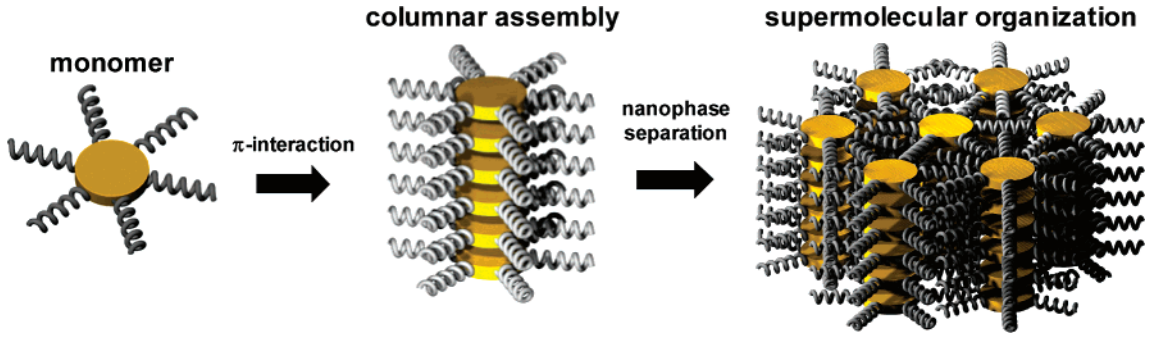

Figure 20. Schematic illustration of the organization process taking place during solidification of alkyl-substituted PAHs from the solution or isotropic phase.

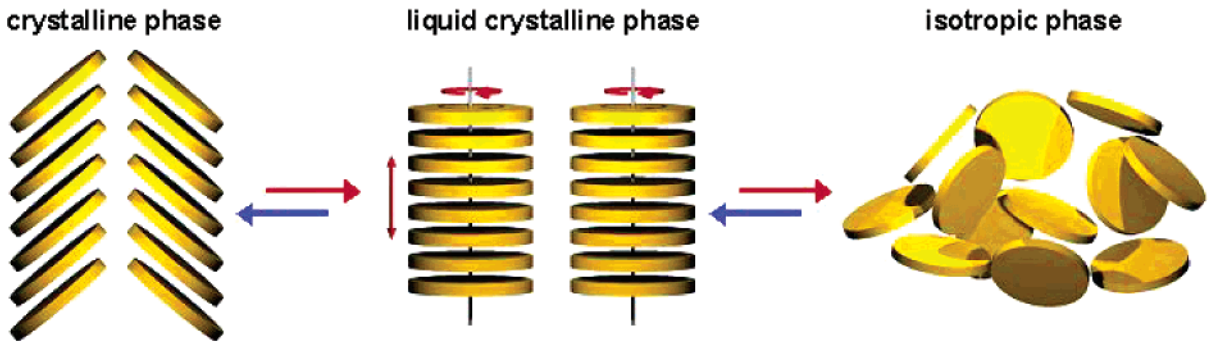

Figure 21. Schematic representation of the organization within the three major phases of alkyl-substituted PAHs.

the most essential bulk parameters for processing. In solution, or in the melt, monomeric species assemble into columns due to π-stacking interactions between the aromatic cores (Figure 20). With higher concentration and/or with decreased temperature, the size of the columnar aggregates in solution increases, resulting ultimately in the solidification of the material. During this final organization process, nanophase separation takes place between the highly ordered, rigid aromatic cores and the disordered aliphatic chains. The overall superstructure contains a columnar organization of disc-shaped molecules (Figure 20), the so-called discotics, which in turn arrange into a two-dimensional array.[84,85] The alkyl side chains fill the intercolumn space. The attached chains increase the overall disorder in the system as well as the heterogeneity between the two nanophases, which has fundamental consequences on the thermal behavior of these materials. Though the nonsubstituted PAHs do not reveal any phase behavior or solubility, the substituted derivatives often show multiple (meso)phases upon heating, depending on the length and bulkiness of the substituents. The thermal phases differ in the degree of supramolecular order and in the dynamics. It is possible to distinguish between three major phases for most discotic HBCs.

In the crystalline state, the molecular mobility of alkyl-substituted PAHs is minimal and the stacking order is high within the columnar structures (intracolumnar).[19a] Typically in this phase, the aromatic cores are tilted with respect to the columnar axes and the side chains are frozen in the disc periphery (Figure 21). In contrast to unsubstituted conjugated molecules or conjugated polymers, discotics reveal an intermediate columnar liquid crystalline phase in which the molecular dynamics increase with higher temperatures. This increased molecular motion leads to lateral and longitudinal fluctuations of the discs accompanied by molecular rotation around the columnar axis (Figure 21).[19a] The high dynamics of the molecules allows a spontaneous self-healing of (structural) defects, which is an important feature of charge transporting materials.[86] At the phase transition from the solid state to the isotropic phase, the columnar structures break

SAMSUNG EX. 1012 - 15/30

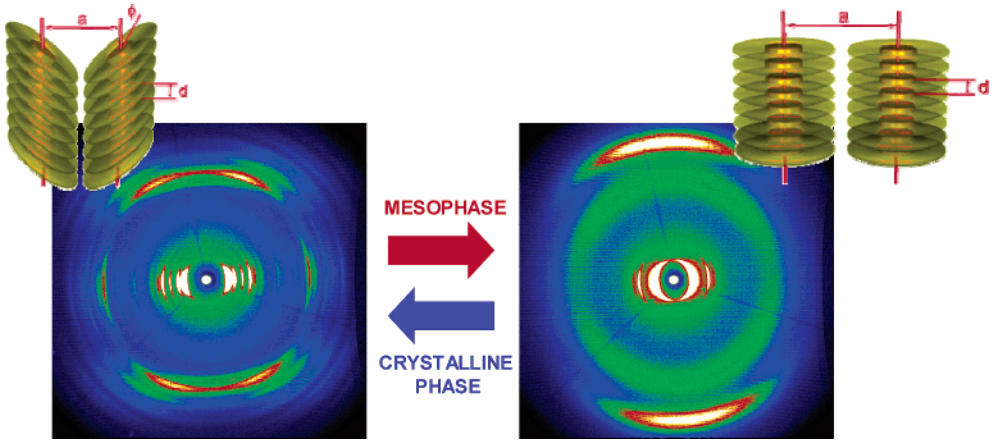

Figure 22. Example of 2D-WAXS patterns and schematic illustrations of the herringbone order in the crystalline phase and the nontilted arrangement in the mesophase for hexadecyl-substituted HBC.

into monomeric species or small aggregates, leading to an amorphous melt.

Detailed investigations are necessary to understand the complex relation between molecular design, self-organization, and thermal behavior. Our structural evaluations indeed have revealed a close correlation of the size of the aromatic core and the type of substituents with the supramolecular organization and the thermotropic liquid crystalline properties. The discotic liquid crystalline phase of the graphene molecules in the bulk state, provoked by the nanophase separation between the rigid π-stacking aromatic cores and the disordered aliphatic substituents, has been studied by a combination of techniques such as differential scanning calorimetry (DSC), polarized optical microscopy (POM), X-ray diffraction,[18] and solid-state NMR spectroscopy.[87]

Two-dimensional wide-angle X-ray diffraction (2D-WAXD) experiments on extruded filaments from plastically deformable phases are extremely useful to understand the supramolecular packing of the discs in the bulk state. An orientation of the columnar structures along the applied shear and the filament axis was observed. Additionally, X-ray measurements were performed at different temperatures to determine the supramolecular organization in different phases as depicted in Figure 22. In general, HBCs substituted by linear alkyl chains self-assemble in the crystalline phase into the "herringbone" order, whereby the aliphatic side chains are phase separated and disordered in the columnar periphery.[19] At the phase transition to the mesophase, the dynamics of the disc-shaped molecules increases accompanied by a change of the columnar arrangement to a nontilted packing of the aromatic cores leading typically to a hexagonal intercolumnar organization.[19] A close relation was found between the hexagonal lattice constant and the aromatic core size or the length of linear side chains.[16] Very fast magic-angle spinning (MAS) solid-state NMR spectroscopic techniques provided detailed information on the molecular packing and dynamics of these disclike molecules in different phases.[88] Thus, distinct aromatic resonances were observed for the hexakis-(*n*-dodecyl)-*peri*-hexabenzocoronene (**HBC-C12**), in the crystalline phase due to different magnetic environments of the symmetry equivalent aromatic protons caused by the ring current effect of adjacent layers; however, in the liquid crystalline phase, axial motion of the HBC discs in the column led to the averaging of the multiple signals into a single resonance.

Columnar stabilization is an important issue for supramolecular engineering and for the improvement of the charge

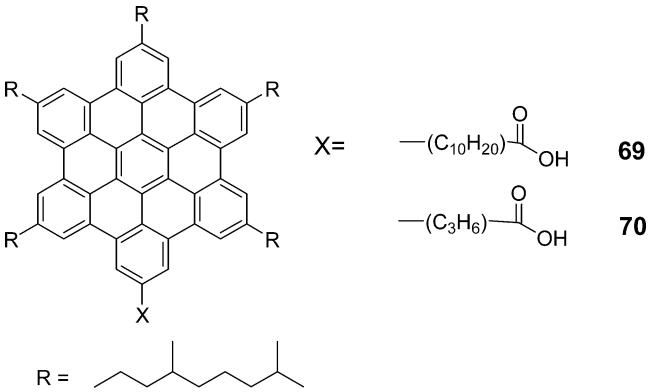

Figure 23. Aliphatic carboxylic acid-substituted HBCs.

transport through the self-assembled columns. One way to enhance the stability of the disc stacking is the introduction of hydrogen bonding by carboxylic acid functions or alcohol groups.[89] HBCs carrying aliphatic carboxylic acids (**69** and **70** in Figure 23) were prepared, and the length of the tethers between the aromatic core and the functional groups plays a crucial role for the prevailing motif.[90]

It has been shown that helical stacking of triphenylenes is related to an improved molecular packing, resulting in higher one-dimensional charge carrier mobilities.[91] The introduction of helicity in systems consisting of larger PAHs requires substituents which possess a much higher steric hindrance. It has been shown that bulky rigid diphenylacetylene arms can induce a rotation of HBC discs (**26b** and **26c**) toward each other (Figure 24).[45b] The molecules were rotated laterally toward each other successively by 15° with a helical pitch of 5 molecules, leading to the formation of a plastic phase.[92] Due to the enhanced molecular packing, the isotropization temperature was not reached before 500 °C, indicating a significantly higher stability of the columnar stacks.

The solution processing of organic semiconductors is one of the most desirable ways to incorporate these materials as thin films in electronic devices. The macroscopic ordering of the molecules can be controlled by the choice of solvent, temperature, concentration, and surface treatment.[93] However, for a successful device fabrication, first it is important to understand the relationship between the molecular architecture and the self-assembly processes in solution and on the surface during solution deposition.

It has been found that derivatives with linear side chains, such as **HBC-C12**, possess a lower solubility and a higher

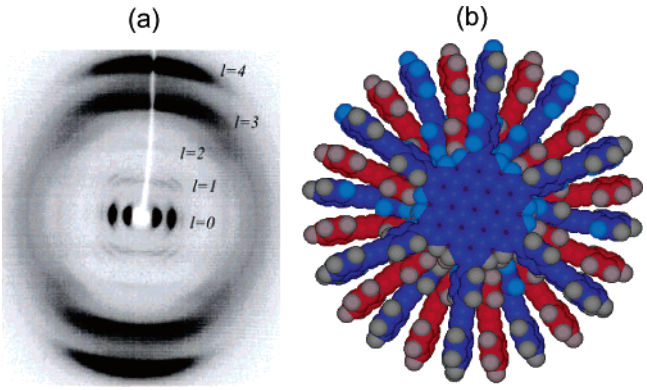

Figure 24. (a) 2D X-ray diffraction patterns for extruded fibers of **26c** at room temperature; (b) proposed helical stacking with each successive disc rotated by 15° about the columnar axis. Every fifth disc is rotationally eclipsed. Alkoxy chains are omitted for clarity. (Reprinted with permission from ref 45b. Copyright 2004 American Chemical Society.)

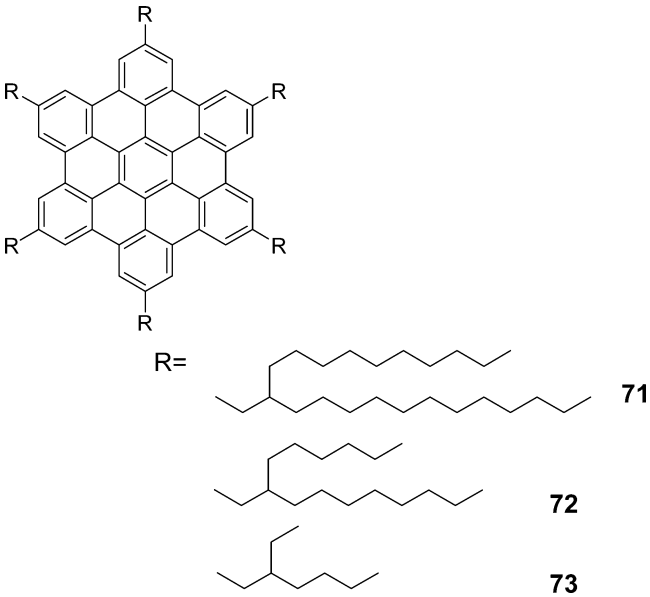

Figure 25. Molecular structures of sixfold branched alkyl chain-substituted HBCs.

self-association constant in comparison to those of derivatives carrying bulky branched alkyl chains **71**−**73** (Figure 25).[94] Long branched side chains hinder the approach of the discs and lead to an increase in the solubility by more than 3 orders of magnitude. Due to the high self-aggregation, **HBC-C12** formed microfibers when drop-cast from the solution independent of the evaporation rate of the solvent (Figure 26a).[29] Structure elucidation showed a columnar organization along these microfibers. In contrast, **73** revealed significantly shorter fibers when drop-cast from solvents such as THF, but centimeter-long, crystalline fibers were obtained for solvents with very low evaporation rates. This behavior revealed the important role of the kinetics of the self-assembly, which followed from the steric requirement of the dove-tailed alkyl substituents (Figure 26b).[29] During dipping at higher concentrations and low solvent evaporation rates, a uniaxial orientation of **73** into surface layers (Figure 26c,d) was obtained.

As briefly mentioned in section 2.1, more complex self-assemblies from solution can be obtained by the introduction of hydrophobic and hydrophilic substituents at the HBC core. The balance between the hydrophobic and hydrophilic nature

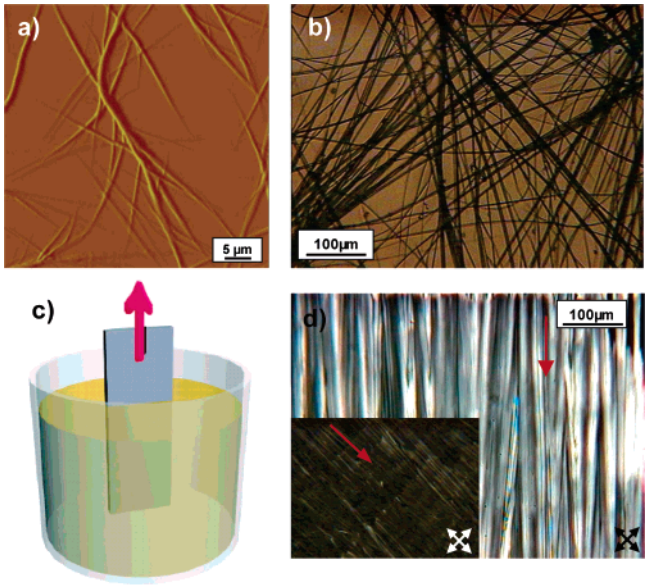

Figure 26. (a) AFM topography of the microfiber morphology (tapping mode) of **HBC-C12**; (b) optical image obtained after evaporation of a **73** solution with a concentration close to saturation; (c) setup for the dipping experiment of **73**; (d) POM of the interior of the film revealing a uniaxial orientation of the microfibers. (Reprinted with permission from ref 94. Copyright 2005 American Chemical Society.)

at one building block is an additional driving force for the superstructure formation. For instance, discrete nanotubular objects have been observed for the amphiphilic HBC **66a** when deposited from solution, which were 14 nm wide, with an open-ended hollow space and a wall thickness of 3 nm.[81a] SEM and TEM experiments revealed that the graphitic nanotubes consisted of helical arrays, established by rolling-up of a 2D pseudo-graphite tape, which in turn composed of a bilayer structure of the π-stacked graphene **66a** molecules.[81a] The alkyl chains were considered to interdigitate and to hold the bilayer structure, whereas the hydrophilic triethylene glycol chains covered the exterior and interior surfaces of the tubes. When the ethylene glycol chains were replaced by two chiral oxyalkylene side chains (**66b**), graphitic nanotubes with one-handed helical chirality were obtained.[81b] The (*R*)- and (*S*)-enantiomers of the amphiphile coassembled at varying mole ratios to give chiral nanotubes with a single helical sense which was determined by the major enantiomer (majority rule).

4. Alignment of Graphene Molecules in Thin Films and Their Device Applications

The very high local charge carrier mobilities detected by the PR-TRMC technique[22] suggest the graphene molecules as very attractive organic semiconductors in electronic devices. However, in thin-film devices, the bulk charge transport is usually limited due to the disorder of the active material deposited between the electrodes, grain boundaries (defects), and metal−interface resistance. Therefore, the control of their supramolecular order over macroscopic dimensions is a key issue to obtain optimized performance. In general, facile fabrication of large areas is a requirement for the production of low-cost electronics. The control of the molecular arrangement on the surface is also an important issue during the discotic material processing. For FETs, an "edge-on" organization of discotics in uniaxially oriented

SAMSUNG EX. 1012 - 17/30

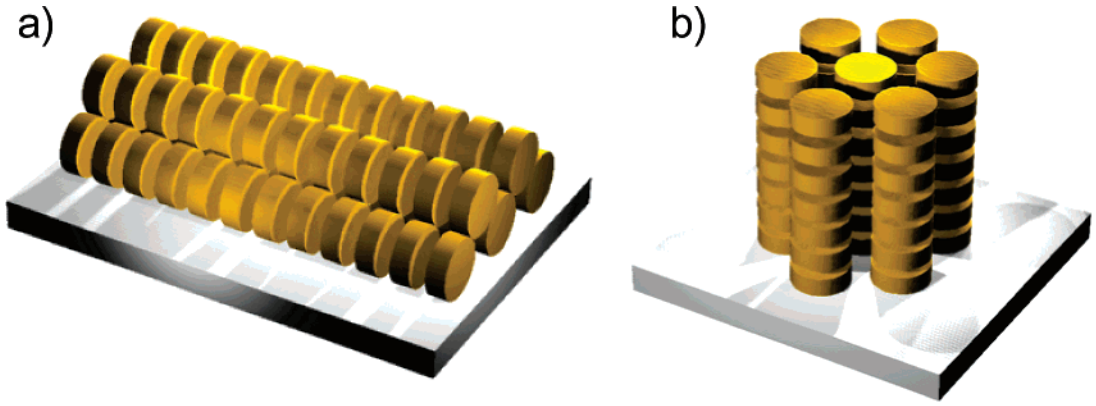

Figure 27. Schematic representation of the different types of supramolecular arrangements on surfaces with (a) edge-on orientation of the molecules, where the columnar axis is oriented parallel to the substrate, and (b) face-on arrangement resulting in homeotropical order. (Reprinted with permission from ref 117a. Copyright 2005 John Wiley & Sons, Inc.)

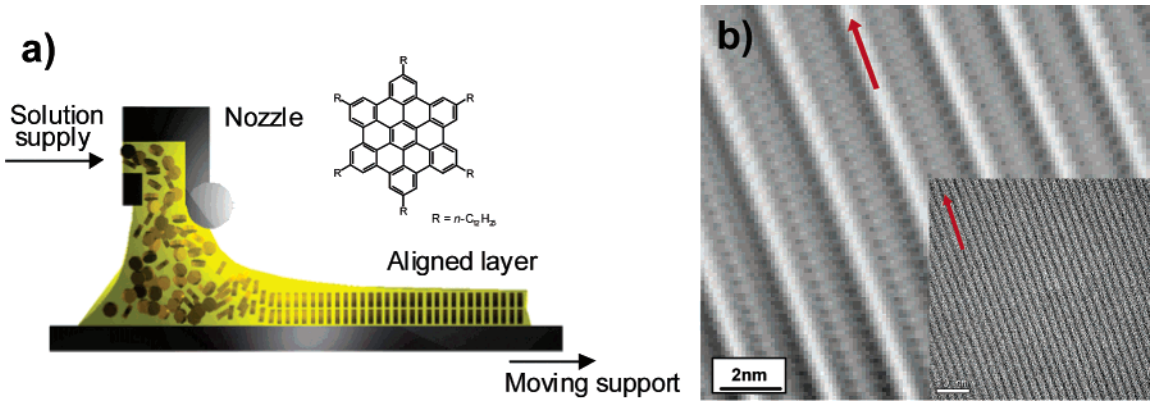

Figure 28. (a) Schematic illustration of zone-cast **HBC-C12**; (b) filtered inverse FFT (IFFT) image showing the intermolecular periodicity within the columns (large area image from HR-TEM displaying a homogeneous film formation with single columnar features oriented in the zone-casting direction). The red arrows indicate the deposition direction. (Reprinted with permission from ref 98. Copyright 2005 John Wiley & Sons, Inc.)

columns is required (Figure 27a). In this arrangement, charge carriers drift through the columns from the source electrode to the drain electrode under controlled gate voltage. In contrast, the large monodomain "face-on" arrangement of the discs leads to a homeotropic phase, which allows faster charge transport between the top and bottom electrodes and favors the photovoltaic performance (Figure 27b). Thus, detailed studies on the control of the supramolecular order and alignment on the surface, leading to device applications, are considered thoroughly in the next section of this review article.

To achieve thin films with a higher macroscopic order from solution, which allowed device fabrication with improved performance, the "zone casting" technique has been shown to be very efficient. As schematically presented in Figure 28a, a solution of organic material is deposited by a nozzle onto a moving support.[95] In this arrangement, a concentration gradient is formed between the nozzle and the support. At the critical concentration, the material is nucleated from the solution onto the moving support as an aligned thin layer. It has been reported that this processing technique is an adequate method for the orientation of polymers with different compositions.[96] In the case of aliphatic chain-substituted PAHs capable of π-stacking, the optimal processing conditions are closely related to the self-aggregation of the molecules in solution.

Using the zone-casting technique, **HBC-C12** was successfully aligned into highly ordered surface layers. The success of the technique is believed to come from the strong self-aggregation and pronounced size of the preaggregates already existing in solution before the deposition. Atomic force microscopy in tapping mode (TM-AFM) revealed pair-packed columnar structures uniaxially oriented in the deposition direction with exceptionally high length exceeding the investigated area.[97] By scan-induced etching of the first monolayers, the underlying layer of stacks became visible and revealed the further pairs of columns in successive layers. The step heights were in accordance with large-area X-ray diffraction in reflection mode. High-resolution transmission electron microscopy (HR-TEM) (inset of Figure 28b) displayed a perfect orientation suggesting a high supramolecular order with edge-on arranged molecules.[98] Additionally, the filtered inverse fast Fourier transform (FFT) image disclosed an obvious intracolumnar periodicity corresponding to the characteristic stacking of the discs (Figure 28b). Electron diffraction and grazing incidence X-ray diffraction of the zone-cast thin layers provided structural information and exhibited a pattern characteristic of a quasi "single-crystalline" supramolecular structure.[99] It was derived that the discs were arranged in the characteristic herringbone order with a molecular tilting angle of ~45° with respect to the stacking axes. Heating the zone-cast film to the mesophase induced a significant change in the optical behavior from near net zero optical anisotropy in the polarized optical microscopy for the crystalline phase to a highly anisotropic medium above the phase transition temperature (Figure 29a).[100] This change was related to the rotation of the discs from a herringbone arrangement, with a tilt angle of 45°, to

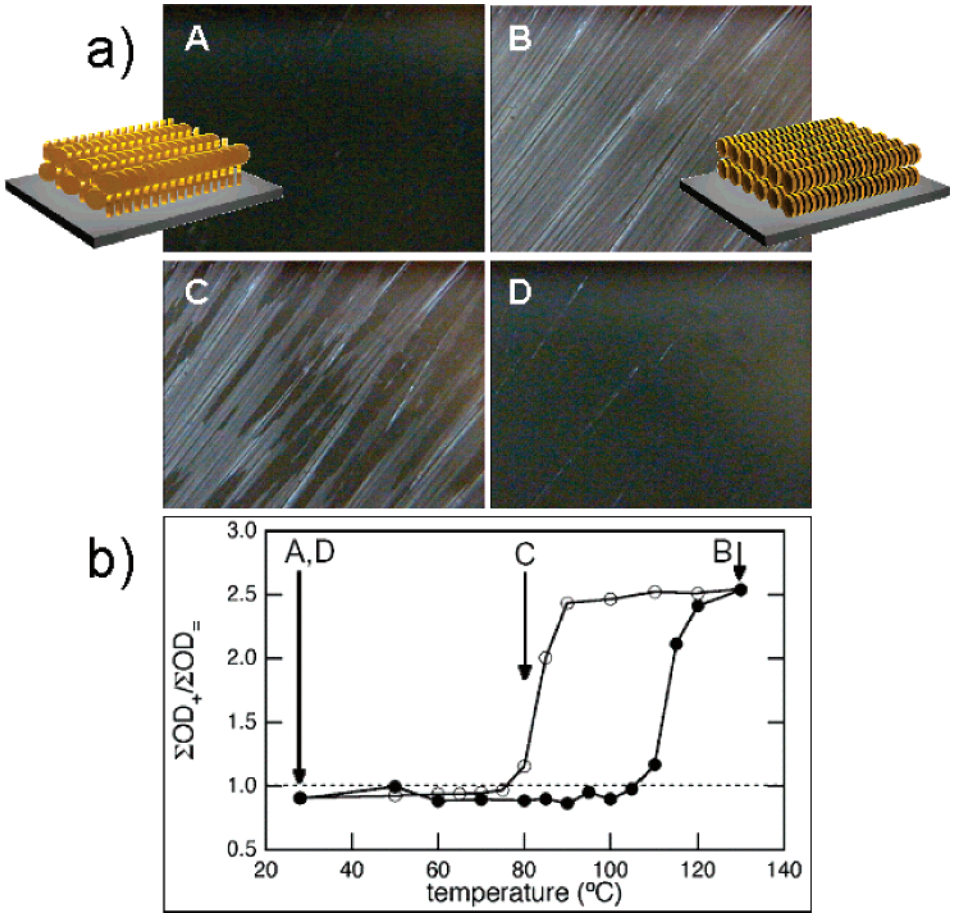

Figure 29. (a) Optical micrographs obtained under crossed polarizers: A, pristine sample at room temperature; B, liquid crystalline phase at 130 °C; C, liquid crystalline phase at close to the phase transition temperature on cooling; D, crystalline phase on returning to room temperature (the insets in A and B present schematically the organization on the substrate in the corresponding phase). (b) Temperature-dependent optical density ratio of a zone-cast film composed of **HBC-C12** at the absorption maximum for the incident light polarized perpendicular and parallel with respect to the casting direction.

the cofacial, nontilted packing.[101] The temperature-dependent evaluation of the dichroic ratio illustrated impressively the reversible change of optical anisotropy that occurred at the phase transition (Figure 29b).[102]

Because **HBC-C12** showed one of the highest local charge carrier mobilities of all discotic liquid crystals (up to 1.1 $cm^2/(V\ s)$ in the bulk state),[22] a fabrication of highly ordered layers of **HBC-C12** over macroscopic areas emerged to be of great interest for the application in field-effect transistors. FET devices based on **HBC-C12** aligned films were constructed with top contacts as illustrated schematically in Figure 30a.[99] The transfer and output characteristics of the devices, which were measured parallel to the columnar alignment, revealed a good on−off ratio of 10^4 and a field-effect mobility in the saturation regime at 5×10^{-3} $cm^2/(V\ s)$ (Figure 30b). The superior device performance was attributed to the highly ordered and uniformly oriented **HBC-C12** resulting from the zone-casting technique. However, it should be noted that the charge carrier mobilities of **HBC-C12** in FETs are still 2 orders of magnitude lower than the mobility values obtained by PR-TRMC. This significant difference can be related to the presence of intracolumnar packing defects, which can constitute localized barriers for charge carrier motion along the columns. Even at low concentrations, these defects can significantly decrease the charge carrier transport over longer distances.

As mentioned already, for industrial low-cost device fabrication, the processing should be as simple as possible. The Nuckolls group reported FET mobilities of just spin-coated **32c** approaching 0.02 $cm^2/(V\ s)$, a threshold voltage of −3 V, and on−off current ratios of 10^6.[49] These values are the most promising field-effect transistor properties achieved so far for a columnar discotic material. Since **32c** is only fourfold substituted by insulating alkoxy groups, the concentration of the active semiconductor in the deposited film is much higher, in comparison to that of the above-mentioned **HBC-C12**. This might be one explanation for a pronounced device performance of **32c**. Furthermore, less disordered side chains attached at the hexa-*cata*-hexabenzocoronene core lead to a stronger interaction between the **32c** molecules in solution and finally to higher macroscopic order, which determines the FET mobility.

In contrast to **HBC-C12,** PAHs such as the hexakis-(4-*n*-dodecylphenyl)-*peri*-hexabenzocoronene (**HBC-PhC12)** and dodecyl chain-substituted C_{96} discs (**C96-C12**, **36a**) possessed an apparently lower self-organization in drop-cast films, indicating a poorer self-aggregation in solution. Additional studies suggested, however, that zone-cast films of both compounds displayed high macroscopic uniaxial orientation of the columns with a molecular edge-on arrangement on the support.[103] Electron diffraction implied a high intracolumnar periodicity, but a low intercolumnar correlation of the discs due to increased molecular dynamics in the liquid crystalline phase (Figure 31). On the other hand, liquid crystallinity allows self-healing of macroscopic defects,

SAMSUNG EX. 1012 - 19/30

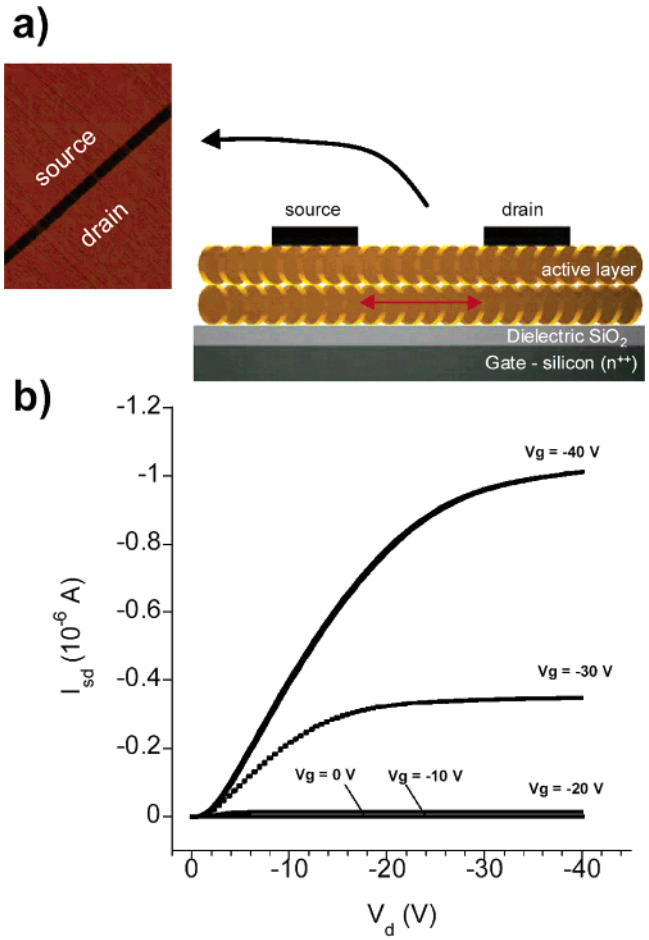

Figure 30. (a) Schematic side-view representation of the top-contact device configuration with contacts evaporated onto the 20 nm thick zone-cast **HBC-C12** aligned film. The discs represent the tilted molecules in edge-on arrangement. The red arrow indicates the charge transport direction. The optical image shows the aligned layer in a 25 μm long channel of a FET. (b) $I-V$ output characteristics of the zone-cast **HBC-C12** as an active layer. (Reprinted with permission from ref 98. Copyright 2005 John Wiley & Sons, Inc.)

making the zone-cast films of these two compounds especially interesting for FET devices.

Another innovative way to macroscopically align **HBC-PhC12** as a thin film by solution processing is the application of a strong magnetic gradient.[104] Using this technique with a horizontal 20 T gradient, a solution of **HBC-PhC12** was cast onto FET wafers. This resulted in large-area monodomain films as proven by POM and X-ray experiments. The HBC molecules were found to be aligned edge-on with their planes along the applied magnetic field, whereas the close-packed columns were oriented ~40° with respect to the gradient. AFM displayed that the thin films consisted of individual "fibers" aligned perpendicular to the magnetic field direction. The exploitation of the layers in FETs showed charge carrier mobilities of 10^{-4} cm^2/(V s) perpendicular to the aromatic planes and 3×10^{-6} cm^2/(V s) parallel to the aromatic planes, which was identical to the case for nonaligned films.

Epitaxial growth on preoriented and friction-deposited poly(tetrafluoroethylene) (PTFE) surface layers has been reported for a large variety of materials. Soluble PAHs such as triphenylenes[105] and HBCs[106] were successfully aligned over large areas. The structure evaluation and investigation of the optical behavior indicated well-aligned HBC films with a parallel orientation of the columnar stacks to the underlying PTFE chains (Figure 32a).[107] Furthermore, the epitaxial organization of the 2D unit cell of the HBC molecules fitted with a certain number of the PTFE chains, as Wittmann had predicated for a successful alignment.[107b] The implementation of the aligned HBC layers in a FET showed promising device performance with mobilities of up to 0.5×10^{-3} cm^2/(V s) and a high anisotropy in conductivity with maximum values obtained for the direction along the columnar alignment (Figure 32b).[106]

The Langmuir−Blodgett (LB) technique (Figure 33), which is one of the most frequently applied alignment methods for triphenylenes and phthalocyanines,[108] has also been established for the orientation of HBCs. For these studies, the HBC molecules were asymmetrically substituted and terminated by a carboxylic acid group to provide the desired amphiphilic character of **69**, **70**, **74**, and **75** (Figures 23 and 34).[109] The molecules formed well-defined LB films when spread from a solution at the air−water interface. Grazing-incidence X-ray diffraction and X-ray reflectivity studies of the LB monolayer revealed two crystallographic phases at room temperature, which depended on the surface pressure applied to the film.

The order in the LB films was improved by the introduction of a polar anthraquinone group as an electron acceptor moiety to the HBC aromatic core (**74**).[110] The Langmuir

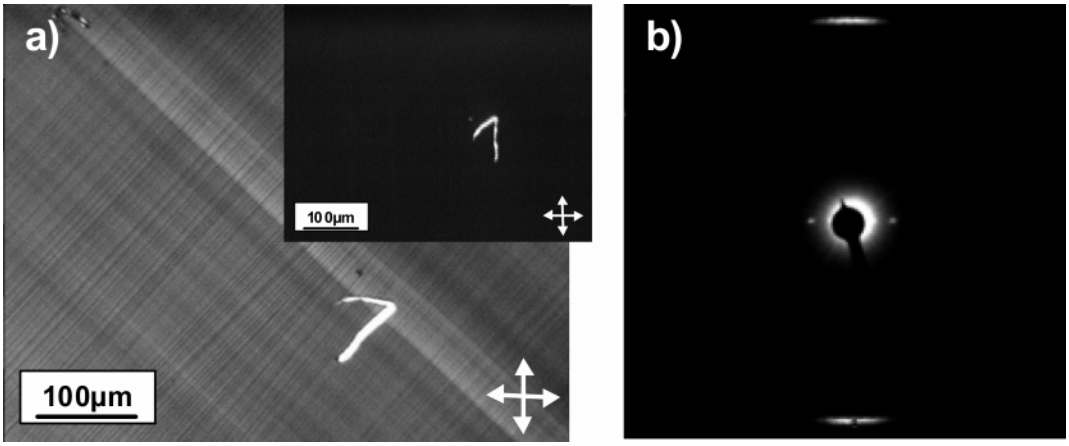

Figure 31. (a) POM images of zone-cast **C96-C12** with 45° (inset 0°) of the deposition direction with respect to the analyzer/polarizer axes (the "1" indicates the same part of the sample and the same light intensity); (b) electron diffraction of zone-cast **HBC-PhC12**. (Reprinted with permission from ref 103. Copyright 2005 American Chemical Society.)

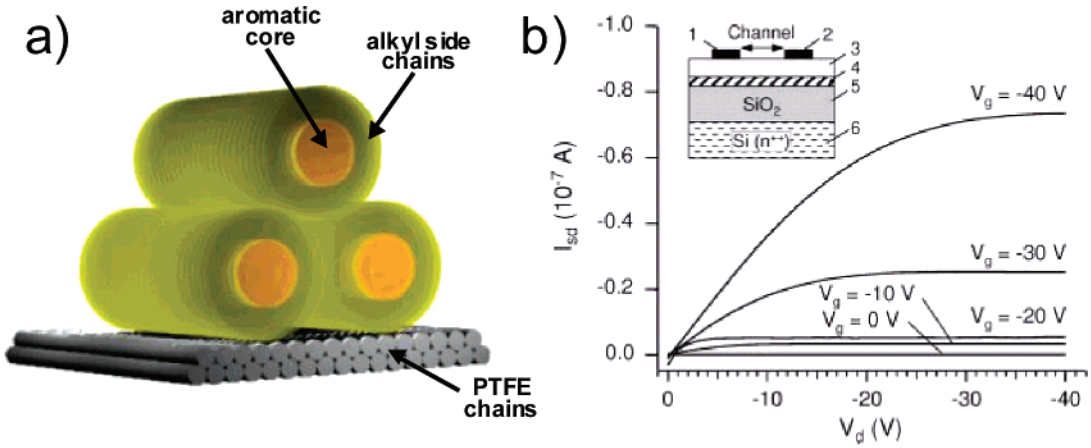

Figure 32. (a) Schematic representation of the columnar HBC stacks lying edge-on and parallel with respect to the underlying PTFE chain; (b) FET device characteristics of an aligned HBC film. (Reprinted with permission from ref 106. Copyright 2003 John Wiley & Sons, Inc.)

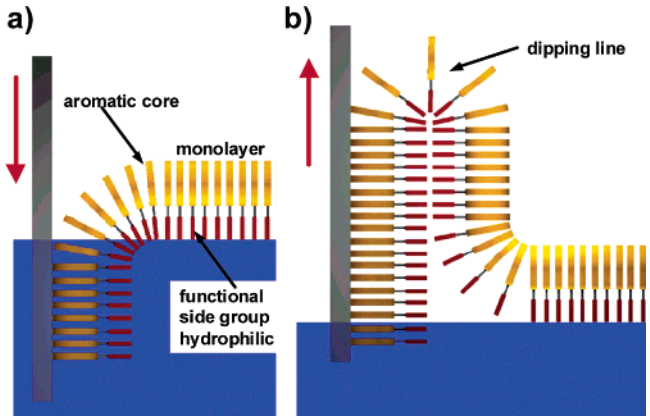

Figure 33. Schematic illustration of the deposition of discotic molecules onto a substrate with the edge-on arrangement using the Langmuir–Blodgett technique.

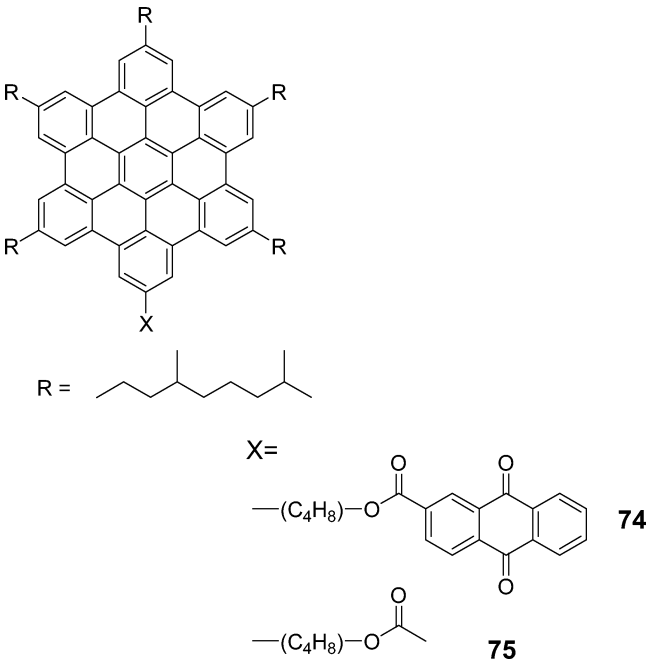

Figure 34. Chemical structures of amphiphilic HBCs.

monolayers at the air–water interface consisted of π-stacked columnar structures with tilted HBC cores relative to the water surface. Efficient transfer of the monolayer to hydrophobic quartz substrates by vertical dipping gave well-defined multilayer films. Thermal processing resulted in an irreversible rearrangement to a single macroscopically aligned phase of hexagonally packed columns. These columns were oriented along the dipping direction with disc planes perpendicular to the columnar axes and stacked in a cofacial manner. Further improvement of the LB alignment was found when poly(ethylene imine) functionalized substrates were used as anchor points for the first layer.[111] The amphiphilic HBC discs formed a macroscopic in-plane orientation of the columns with their main axis parallel to the dipping direction.

For thermal processing, it is necessary to decrease the isotropic phase transition temperature (T_i), which is above 400 °C for HBC derivatives substituted by linear alkyl chains.[27a] The introduction of branched side chains with a high steric demand at the core periphery not only increased the solubility as described above, but also lowered the T_i dramatically. The T_i values for **71** and **72** dropped to 46 and 97 °C, respectively, and therefore opened the opportunity for processing the materials from the isotropic phase.[112] The branching site at the core vicinity along with the high rotational freedom of the alkyl chains played a key role in lowering the transition temperature. According to the behavior in solution, the self-organization during crystallization was strongly affected by the steric requirements of the side chains. The increased side chain length resulted in the formation of larger ordered domains.[113] Spherulitic domains of **71**, in which the columnar structures were oriented radially, with sizes extending over 4 mm in diameter were found and indicated the high degree of self-organization over long ranges (Figure 35a), whereby the columnar growth of **72** took place around the nucleation center (Figure 35b).

Due to this extraordinary directed growth, **71** has been successfully aligned by zone-crystallization (Figure 36a).[114] The sample was moved at a defined velocity from a hot plate with a temperature above the isotropic phase to a cold plate with a temperature lower than T_i. Between these two plates, the material crystallized along a temperature gradient as an aligned film. Indeed, after zone-crystallization, two-dimensional wide-angle X-ray scattering (2D-WAXS) revealed a columnar growth along the temperature gradient with edge-on arranged discs. POM also displayed high optical anisotropy characteristic for a macroscopically oriented layer (Figure 36b).[115] A closer inspection by AFM showed a lamella morphology of the film, whereby these lamellae were also oriented in the moving direction of the sample.

SAMSUNG EX. 1012 - 21/30

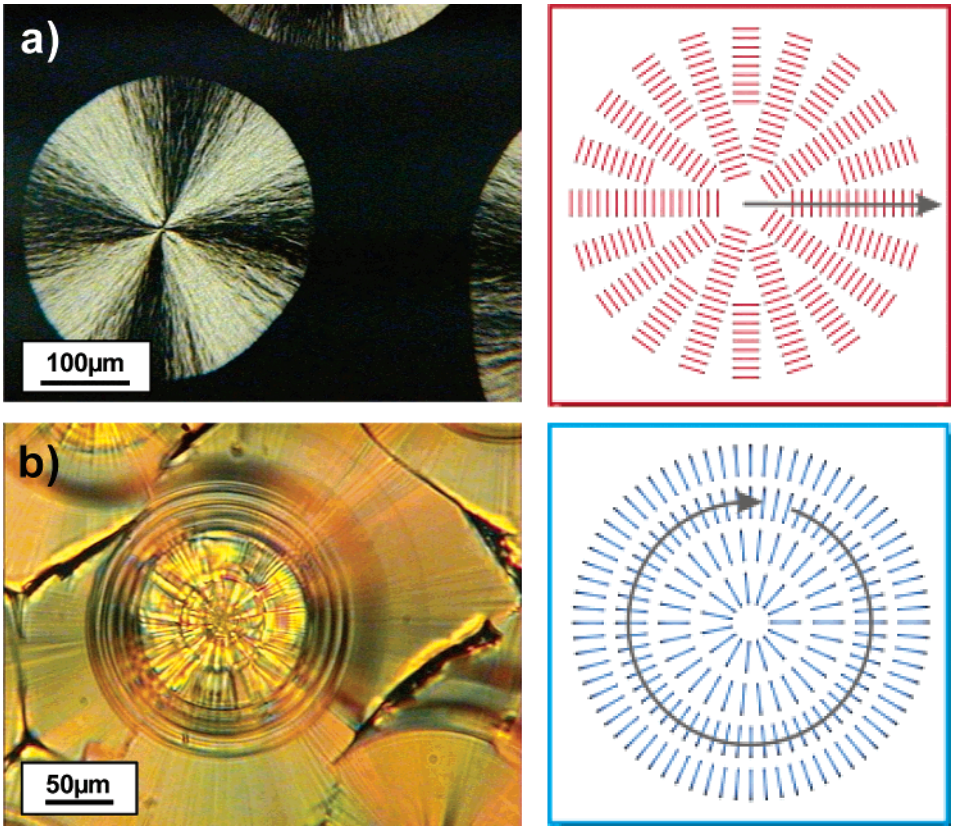

Figure 35. Image from polarized optical microscopy displaying (a) spherulitic morphologies of **71** with the radial columnar orientation and (b) "scalelike" textures of **72** with columnar growth around the nucleation center. Both morphologies were obtained during cooling from the isotropic phase. (Reprinted with permission from ref 113a. Copyright 2006 John Wiley & Sons, Inc.)

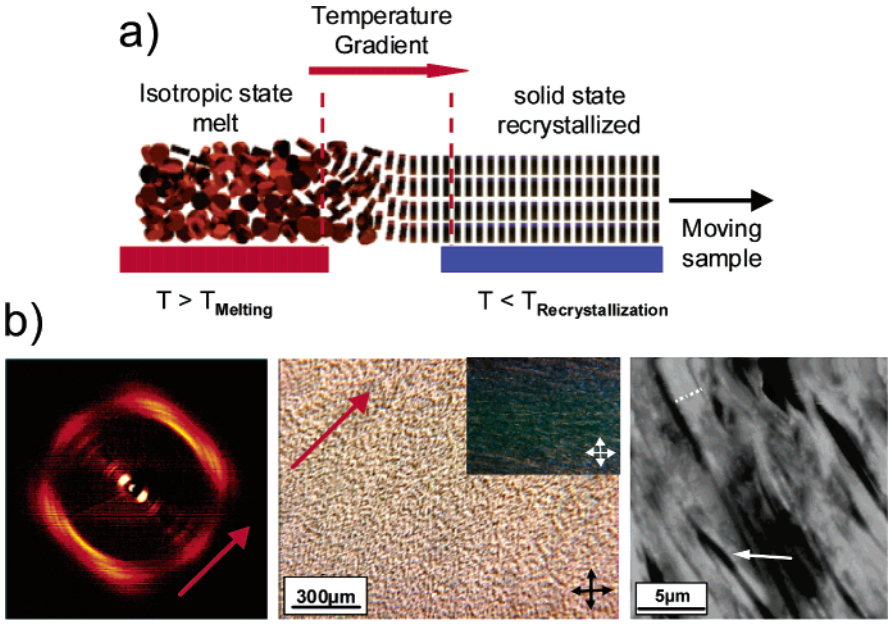

Figure 36. (a) Schematic illustration of the zone crystallization of HBC discs; (b) 2D-WAXS, POM, and AFM of the aligned **71** film. (Reprinted with permission from ref 115a. Copyright 2004 American Chemical Society.)

Since in a photovoltaic cell the active material is "sandwiched" between two electrodes, a homeotropic alignment with graphene discs in a "face-on" arrangement might provide an undisturbed pathway for charge carriers between the anode and cathode and thus might enhance the device performance. It has been reported that the introduction of heteroatoms at the vicinity of a phthalocyanine core increased the affinity of the molecule toward polar surfaces and therefore enhanced the face-on arrangement.[116] HBC derivatives **76**−**79** (Figure 37) showed a spontaneous formation of a homeotropic phase even at very rapid cooling rates. The HBCs were substituted by long branched side chains with ether linkages, which ensured an accessible isotropization temperature for the processing and a sufficient propensity to polar surfaces.[117] The dendritic morphology obtained by cooling the sample from the isotropic phase between two

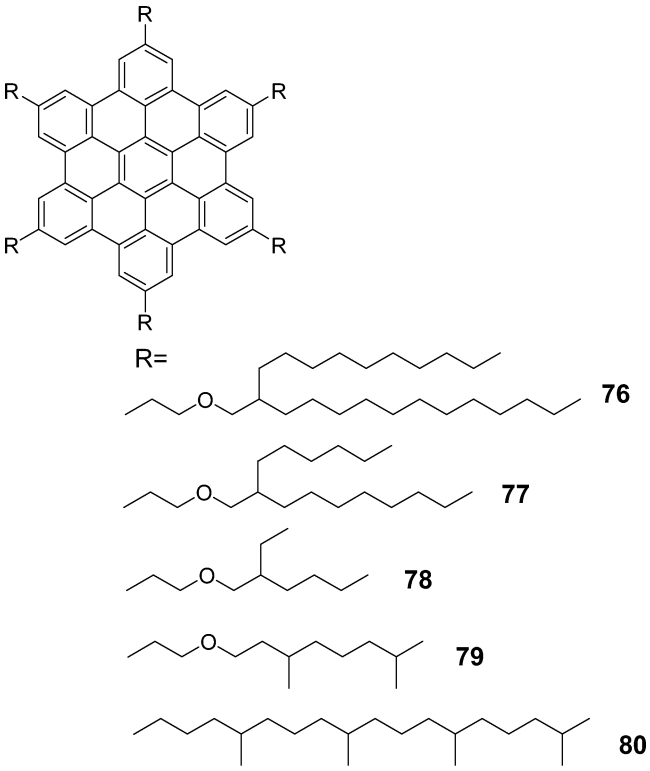

Figure 37. Chemical structures of HBC derivatives which homeotropic alignment.

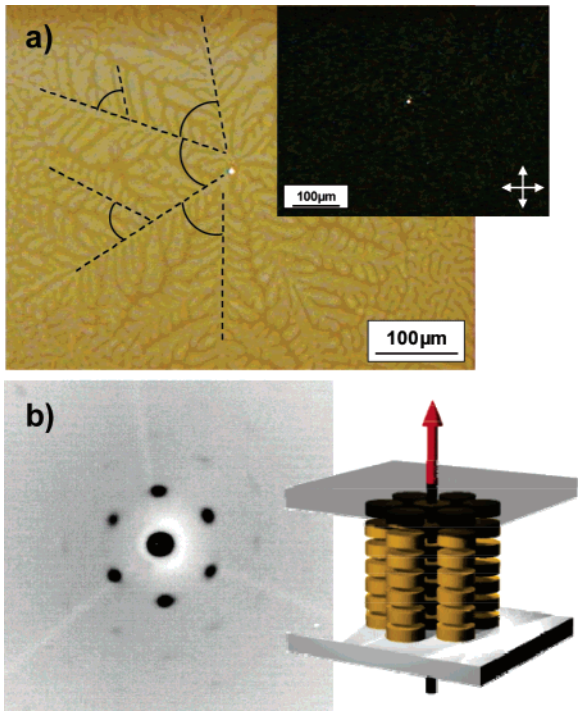

Figure 38. (a) Optical microscopy of a homeotropically aligned sample (inset in cross-polarizers); (b) 2D-WAXS of a homeotropic sample (inset: schematic illustration of a columnar alignment toward the incident X-ray beam). (Reprinted with permission from ref 106. Copyright 2003 John Wiley & Sons, Inc.)

surfaces appeared black via POM, which is characteristic for homeotropic alignment (Figure 38a).[117] 2D-WAXS confirmed the columnar orientation over large areas as a typical hexagonal pattern (Figure 38b). Moreover, it was possible for the first time to obtain this specific alignment also on only one surface. The self-organization of the discs on one surface was strongly dependent on the film thickness. For thicker films, random nucleation occurred within the bulk and produced defects.

It should be pointed out that the homeotropic alignment is not limited to derivatives bearing polar linkages. The successful orientation of the all-hydrocarbon **80** indicates that another mechanism might be responsible for the face-on arrangement of the molecules.[118] It is assumed that the homeotropic alignment is thermodynamically favored and therefore the most probable ordering of discotics toward the surface. The short-circuit photocurrents of aligned areas of **80** were significantly higher in comparison to those of areas with poor orientation, indicating that the homeotropic phase can enhance the performance of photovoltaics.

On the other hand, a successful performance of a solar cell requires a variety of additional parameters. When a mixture of **HBC-PhC12** and perylene diimide (PDI) was spin-coated from solution, a controlled phase separation was obtained. The mixture produced vertical layers of both compounds that were separated by a rough interface and therefore led to a large surface contact area between the materials.[119] Due to this specific morphology, a photovoltaic cell with very high efficiency and an external quantum efficiency as high as 34% at a wavelength of ~490 nm was found.

The key issues for the production of (high-performance) electronic devices, by means of a targeted synthetic approach and physical processing, are the control of the order and alignment of discs in bulk thin films. The self-assembly of discs at interfaces is also of great importance because it relates to the charge carrier transport at organic molecules/substrate interfaces and also opens the opportunity to fabricate molecular scale electronics. In the following part, scanning tunneling microscopy (STM) studies on the self-assembled monolayer or double layers at the solid−liquid interfaces will be described.

5. Self-assembly at Solid–Liquid Interfaces

STM, angle-resolved X-ray photoelectron spectroscopy, and low-energy electron diffraction (LEED) studies on vacuum deposited HBC thin films revealed that the HBC discs displayed an epitaxial growth with an ordered face-on arrangement on HOPG, Au(111), MoS_2, and Cu(111) surfaces.[120] The unique face-on arrangement of discs suggests strong interactions between the large π-surface and the substrates. The alkyl-substituted or parent graphene molecules also showed ordered growth of 2D crystals on the HOPG or Au(111) surfaces as probed by STM. The strong van der Waals interactions between the substrates and graphitic discs, as well as alkyl chains, induce ordered monolayers or bilayers at the solid−liquid interface.[121]

Alkyl-chain-substituted HBCs (e.g., **HBC-C12**) formed regularly arranged monolayers on the HOPG surface in solution (Figure 39a) and produced asymmetric *I*/*V* characteristics when measured by scanning tunneling spectroscopy.[27a,122] The alkyl chains were found to be arranged along the main axes of the graphite substrate (inset in Figure 39a). When graphite was modified by *n*-pentacontane (n-$C_{50}H_{102}$) adsorption layers, structural phase transitions with formation of time dependent α-, β-, and γ-phases ($\alpha \rightarrow \beta \rightarrow \gamma$) were observed for absorbed **HBC-C12** at the *n*-tetradecane−solid interface.[122] The initial α-phase is similar to that obtained on bare graphite while intermediate β- and final γ-structures present molecular dimers and rows, re-

SAMSUNG EX. 1012 - 23/30

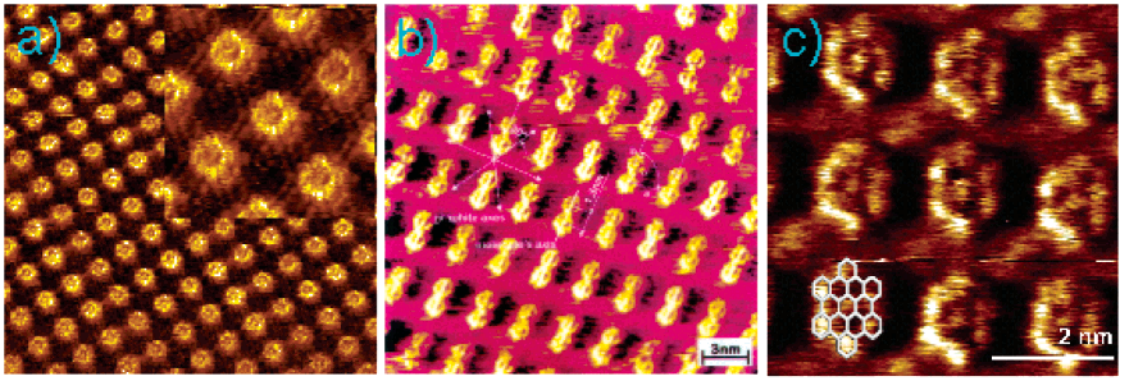

Figure 39. STM images of **HBC-C12** (a), **44** (b), and parent HBC (c) on an HOPG surface. (Reprinted with permission from refs 122 and 124. Copyright 2005 and 2000 American Chemical Society.)

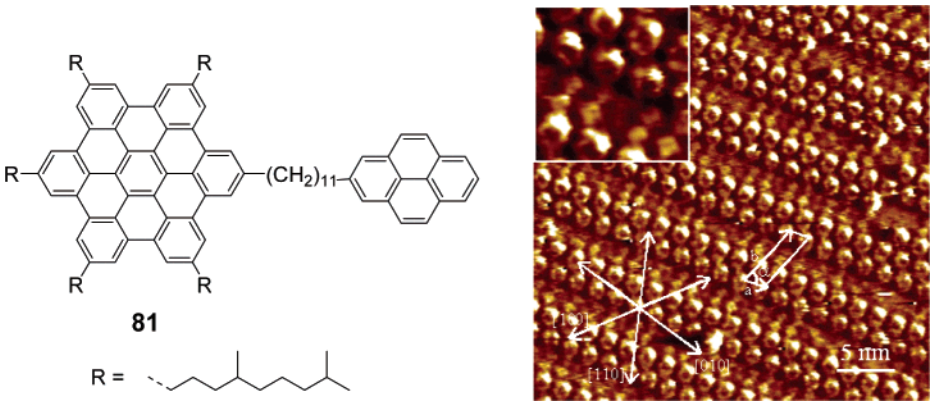

Figure 40. Molecular structure of compound **81** and STM images of the monolayers adsorbed on an HOPG surface. (Reprinted with permission from ref 126. Copyright 2003 American Chemical Society.)

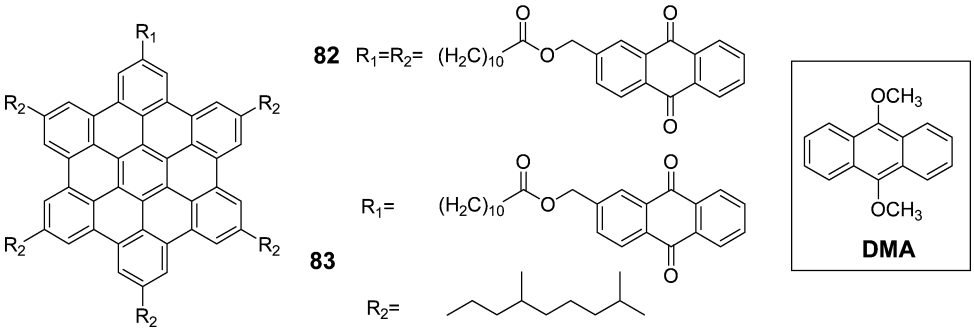

Figure 41. HBC molecules substituted by electron acceptor anthraquinones.

spectively. Such two-dimensional polymorphism is due to weak interactions between **HBC-C12** molecules and the alkane-modified graphite substrate. The alkylphenyl-substituted HBCs self-assemble into 2D crystals of the discs with variable vertical displacements from the substrate.[123] When the alkylphenyl chains contain chiral centers, a regular staircase superstructure was observed. A submolecular visualization of a covalently linked HBC dimer (**44**, R = $C_{12}H_{25}$) on the HOPG surface revealed a contrast, which reflects the structure of the aromatic parts of the molecule, with the aromatic moieties being oriented like graphene layers in graphite (Figure 39b).[124] Processing of negligibly soluble discs such as parent HBC and C132 (**37**) is very difficult. However, epitaxial layers of these unsubstituted discs with electron acceptors can be obtained by self-assembly from "solution", and submolecular resolution was achieved (Figure 39c).[125]

Attachment of other electronic components onto the HBC core and the self-assembled side-by-side monolayers of such dyads provides opportunities to fabricate single molecular devices at the solid−liquid interface. The covalently tethered HBC and pyrene units (e.g., **81**) coassemble to form stable nanophase-separated arrays (Figure 40).[126] The STM current image clearly reveals a 2D crystalline dimer structure, and the bright spots can be attributed to the HBC π-conjugated cores. A careful inspection reveals smaller bright spots tightly packed near the HBC cores (inset), and this feature can be ascribed to the pyrene moieties.

One or six anthraquinone (AQ) electron acceptors were also attached to the HBC core by aliphatic chains (**82** and **83** in Figure 41). These donor−acceptor dyads self-assemble at the solution−graphite interface into either defect-rich polycrystalline monolayers or extended 2D crystalline domains, depending on the number of tethered AQs.[127] The STM studies on the self-assembled monolayer of HBC **82** substituted with six AQs revealed different tunneling behavior of the AQs and HBC subunits. There is an opposite rectifying effect of the HBC core and anthraquinones within

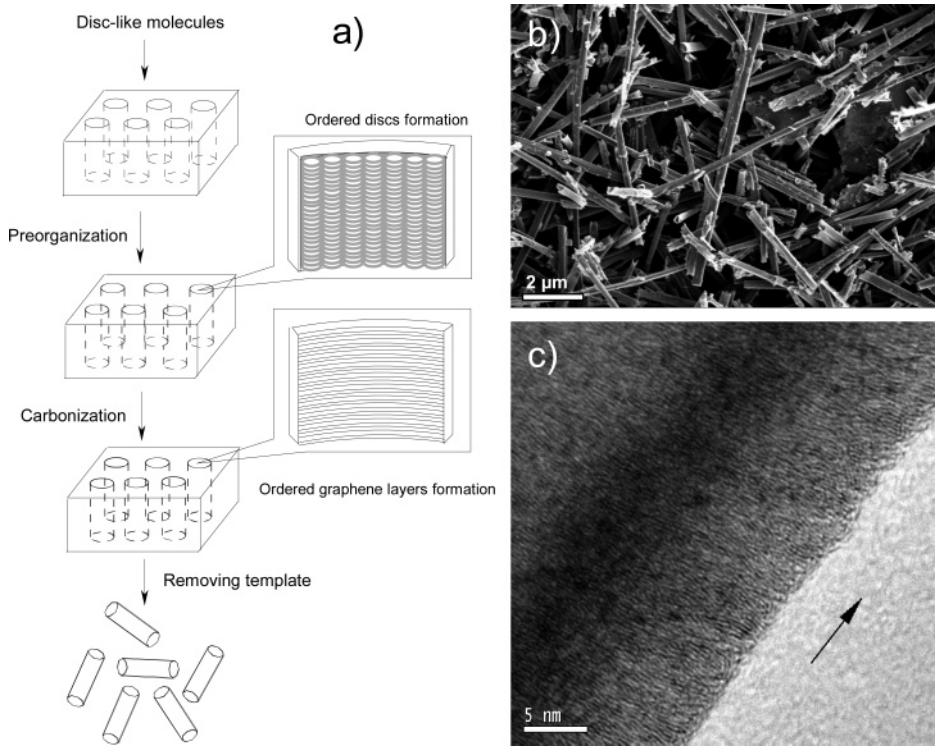

Figure 42. (a) Scheme toward carbon nanotubes by a template method; (b and c) SEM and TEM images of the obtained carbon nanotubes after removal of the template. (Reprinted with permission from ref 132b. Copyright 2005 John Wiley & Sons, Inc.)

the tunneling junction, making these monolayers inversely biased rectifiers, where one of the electrodes is always the STM tip. The different asymmetric tunneling can be explained by resonantly enhanced tunneling through the HOMO and LUMO of HBC and AQ, respectively. When an electron donor such as dimethoxyanthracene (DMA) is added to the solution, a charge-transfer complex between the anthraquinones and DMA is formed at the interface and the current−voltage characteristics through a single molecule in an STM junction are modified.[128] This effect can be explained by a relative shift between the Fermi levels of the substrate and the molecular orbitals of the adsorbates due to the formation of a dipole at the interface. This setup can be viewed as a chemical field-effect transistor (CFET) based on a single molecule with an integrated nanometer-sized gate, since the charge-transfer complexes, which are responsible for the change in $I-V$'s, are formed between an acceptor covalently bound to the molecule in the tunneling junction and a donor coming from the ambient solution. This proof of principle is a step toward molecular scale electronics and highly sensitive electronic molecular probes.

6. Novel Carbonaceous Nanostructures by Solid-State Pyrolysis

The facile formation of ordered columnar superstructures from these graphene molecules in the bulk state and their high stability in the mesophase qualify them as precursors toward novel carbon nanostructures. Therefore, pyrolysis under controlled conditions may maintain the order existing in the mesophase during the formation of the carbonaceous materials. Pitch, which is a mixture of graphitic molecules with different sizes, has been subjected to solid-state pyrolysis with and without templates, and carbon materials with partially graphitic structures have been obtained.[129] Toward a better control of the order, the above well-defined graphene molecules were thus used in solid-state pyrolysis.[130]

Pyrolysis of well-defined graphene molecules in the bulk-state produced novel carbon nano- and microstructures.[131] The graphene molecules such as **HBC-C12** were first heated in the mesophase to around 400 °C, which resulted in the cleavage of alkyl chains while keeping the columnar superstructures, and then carbonized at higher temperature (max 800 °C), yielding larger graphitic nano- and microstructures. The temperatures are much lower than the normally used graphitization temperatures (2000−3000 °C). Recently, a template method has been used to fabricate uniform carbon nanotubes by pyrolysis of graphitic molecules in porous alumina membranes.[132] The graphene molecules were introduced into nanochannels within the alumina template by a simple wetting process[133] and then subjected to carbonization at various temperatures. During the wetting, the graphene molecules aligned along the channels and kept the order under the slow heating procedures. After the template was removed, uniform carbon nanotubes with ordered graphene orientations were obtained in quantitative yield (Figure 42). Interestingly, the orientation of graphene layers is perpendicular to the tube axis due to the preorganization of the disclike molecules in the templates. This is different from the case of normal carbon nanotubes, in which the graphene layers are parallel to the tube axis. Such a template method was subsequently applied to the fabrication of other carbon nanotubes/nanorods using different PAH precursors.[134]

Instead of using graphitic discs in the alumina templates, two tetraphenylcyclopentadienone molecules with acetylene groups (**84** and **85**, Figure 43) were filled into the nanochannels. Subsequent heating at low temperature (250−350 °C) resulted in hyperbranched polyphenylene nanotubes formed by Diels−Alder polymerization reactions between the cyclopentadienone units and the acetylene groups (Figure 43). The tubes formed from **85** are highly flexible due to the flexible aliphatic spacers between the polyphenylene dendron

SAMSUNG EX. 1012 - 25/30

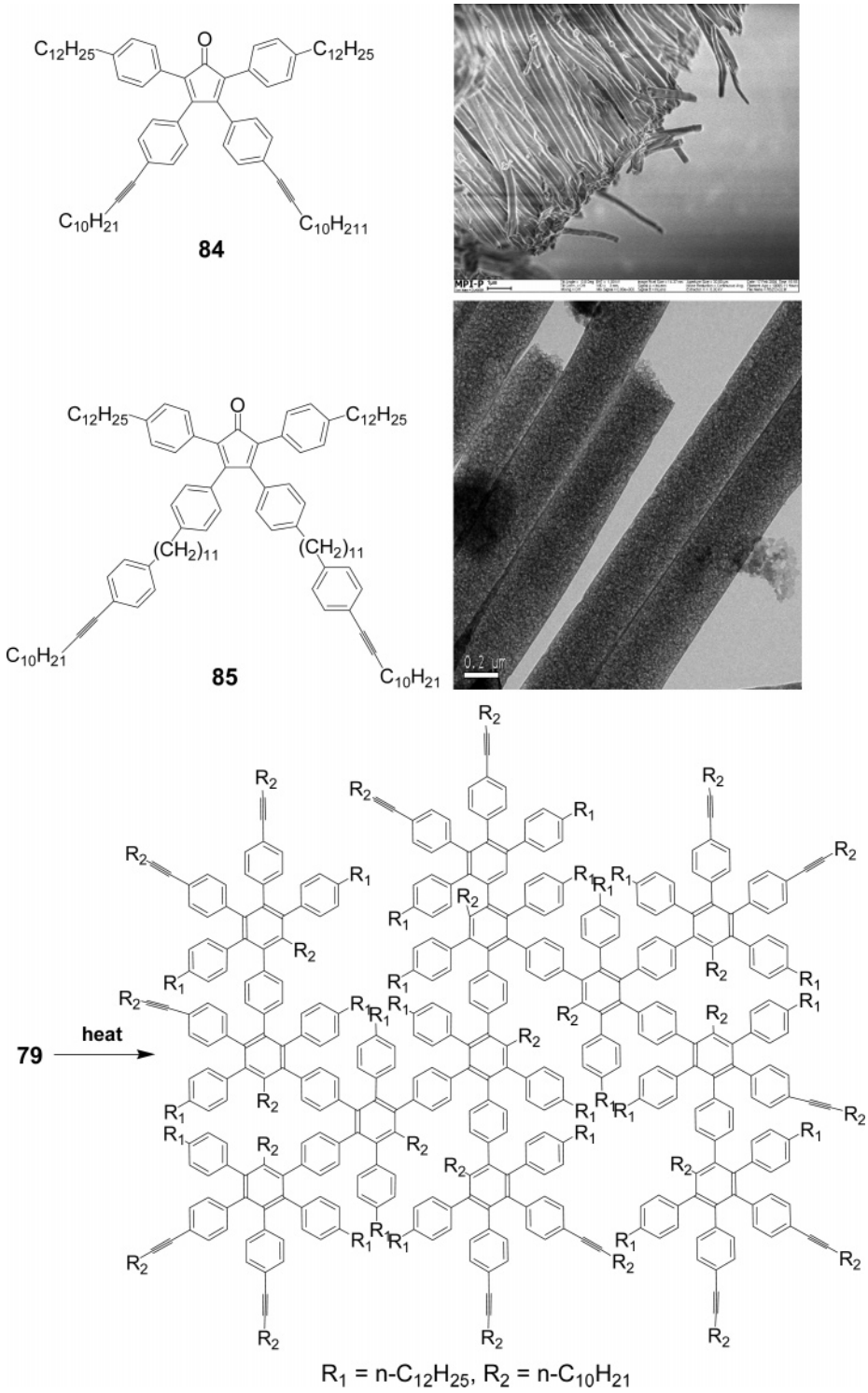

Figure 43. Molecular structures of AB_2-type monomers (**84**, **85**) and the obtained hyperbranched polyphenylenes after Diels−Alder cycloaddition reactions. SEM and TEM images of the carbon nanotubes are also included. (Reprinted with permission from ref 135. Copyright 2005 John Wiley & Sons, Inc.)

units. Carbonization at higher temperature (e.g., 600 °C) led to carbon nanotubes with porous wall structures (Figure 43).[135] These unique porous carbon nanotubes may allow metal catalyst deposition into the pores and gas storage.

Electronic arc-discharge, laser ablation, and chemical vapor deposition have been used in the synthesis of carbon nanotubes and other carbon nanostructures; however, the control of the purity and separation of the products is always a key problem.[32] Controllable solid-state pyrolysis of organometallic precursors recently emerged as an alternative method for preparing carbon nanostructures such as CNTs and carbon onions.[136] Thereby, the organometallic complexes served as the catalyst precursors and as carbon sources for the pyrolysis that was carried out not in the gas-phase but in the solid state at "low" temperature. Vollhardt's and Bunz's groups performed solid-state pyrolysis of several metal-dehydro[*n*]annulene complexes, and a mixture of carbon nanostructures such as carbon onions, tubes, graphite, and amorphous carbons was obtained.[136] Recently, it was found that pyrolysis of the complexes between the diphe-

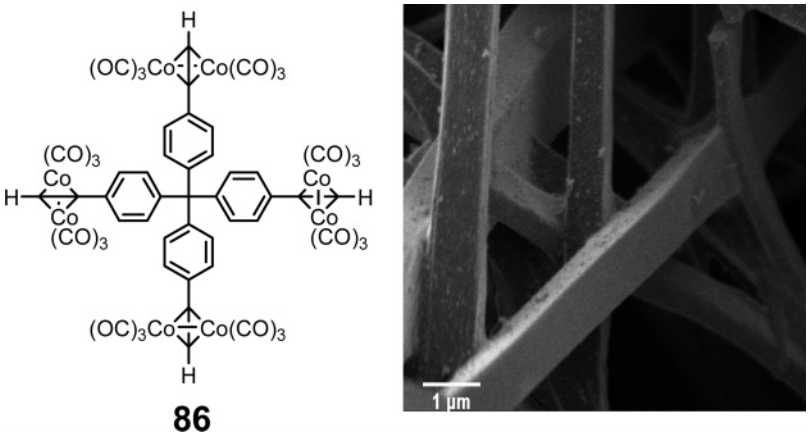

Figure 44. Molecular structure of a tetraphenylmethane−Co complex and SEM image of the uniform nanorods obtained after solid-state pyrolysis. (Reprinted with permission from ref 139. Copyright 2005 John Wiley & Sons, Inc.)

nylacetylene and $[Co_2(CO)_8]$ afforded carbon nanotubes in high yield.[137] The choice of the organometallic precursor appears as the key issue for controlling the morphologies (shape and uniformity) of the carbon structures and the conversion yield. We choose large graphitic disclike molecules, such as HBC, instead of using small hydrocarbons as carbon sources. Thermolysis of the HBC−cobalt complexes[138] in the solid state afforded multiwalled CNTs in nearly quantitative carbon conversion yield. The $[C_2Co_2(CO)_6]$ clusters decomposed during heating and produced well dispersed Co catalyst, and further heating led to carbon nanotube growth from graphitic discs. Depending on the temperature, either "bamboo"-shaped or straight carbon nanotubes were selectively prepared.

Solid-state pyrolysis of different organometallic precursors has been performed to prepare novel carbon and carbon−metal nanostructures, and a simple tetraphenylmethane−Co complex (**86**, Figure 44) was found to be an interesting precursor. Thermolysis of this molecule under a fast heating rate to 800 °C and holding at this temperature for 8 h yielded carbon/Co nanorods with unique rectangular cross sections in high yield (Figure 44).[139] Such rod structures even existed during the "explosive" decomposition at 130 °C. The nanorods consisted of well-dispersed Co nanoparticles surrounded by amorphous carbons. Under a slow heating process, however, carbon nanotube growth from the rods was observed, suggesting that the rods can be regarded as feedstocks of both carbon sources and catalyst.

Carbon-based feedstocks are commonly used as anode materials in lithium batteries given their low density as well as their capability to reversibly incorporate guest molecules such as alkali metal ions. The lithium storage capacity of commercial cells based on graphite anode materials is limited to 372 mA h g^{-1}, associated with its maximum LiC6 stage.[140] To make efficient carbonaceous materials for anodes, we proposed a new concept of using three-dimensional (3D) graphitic materials prepared from controlled solid-state pyrolysis of well-defined carbon-rich phenylene molecules such as hexaphenylbenzene and hexa(4-bromophenyl)benzene (**9**, R = H and Br, respectively).[141] During the heating process, intermolecular aryl−aryl and intramolecular cyclodehydrogenation took place and afforded disordered carbon materials. Electrochemical measurements in lithium cells revealed a stable, high capacity of the order of 600 mA h g^{-1}, which is much higher than those of commercial cells based on graphite. Thus, this concept will be extended to less expensive precursors in the future.

In summary, solid-state thermolysis of graphene molecules with or without templates gave novel carbon nanostructures with ordered graphitic layers that arose from the ordered columnar structures in the mesophase. The inclusion of organometallic clusters in the precursor led to high-yielding solid-state synthesis of carbon nanotubes. An extension of 1D and 2D carbons to 3D graphitic structures resulted in a wide range of carbon nanomaterials for power source applications.

7. Conclusion and Outlook

The synthesis, self-assembly, and device applications of nanosized graphene molecules, and their conversion to novel carbonaceous materials have been introduced. Effective oxidative cyclodehydrogenation of branched oligophenylenes affords well-defined graphene molecules with different shapes, sizes, and edge structures. Moreover, transition metal-catalyzed coupling reactions broaden the family of 2D graphene discs, allowing a precise structural tuning of their thermal properties and supramolecular order in bulk. The alignment of these disclike molecules in fibers and thin films was well controlled by a series of processing techniques such as mechanical extrusion, zone-casting/refining, aligned substrate, magnetic field alignment, and thermal annealing. The performance of these aligned films in electronic devices is much better than that from randomly spin-/drop-cast films. The ordered self-assembly of these disclike molecules at the solid−liquid interface offers the opportunity to fabricate molecular scale electronic devices based on well-arranged functional units. These graphene molecules can also be converted into 1D carbon nanotubes with well-controlled graphene layer orientation under a template-directed solid-state pyrolysis process. In addition, solid-state pyrolysis of these graphene molecule−Co complexes led to multiwalled carbon nanotubes in high yields.

To broaden the scope of these disclike graphene molecules in the future, the size and shape are still issues, and one may also proceed from all-benzenoid PAHs to hydrocarbons with active "zigzag" edge structures, from planar structures to nonplanar (e.g., bowl-shaped) structures, and from all-carbon to heteroatom-containing hydrocarbons. For these variations to become realized, further improvement of synthetic strategies needs to be addressed. The future of using graphene molecules in electronics or photonics depends on improvement of the intrinsic charge carrier mobilities, control of supramolecular order in thin films, and device fabrication

SAMSUNG EX. 1012 - 27/30

processes. These requirements suggest a joint activity of chemists, physicists, and engineers. Further miniaturization of devices to molecular scale is possible; however, the key issue is how to integrate and assemble different electronic elements into ordered nanostructures. Carbonization of the graphene molecules provided good control of the structures and electronic properties of obtained carbon materials. The obtained semiconducting tubes can be used in field-effect transistors. In addition, chemical modification of the peripheries of these special carbon nanotubes or filling foreign materials in the pores may lead to complex nanostructures for electronic applications.

Finally, it is worth noting that, in contrast to our "bottom-up" design of well-defined graphene molecules, Haddon et al. very recently reported a "top-down" approach toward soluble graphene materials.[142] Under strongly oxidizing acidic conditions, similar to the functionalization of carbon nanotubes, microcystalline graphite was converted to graphite oxide, which was further functionalized by long-chain alkylamine to give rise to stable solutions of these materials in organic solvents. Charge transport measurements on a few layers of graphene or even single layer graphene suggest great promise in electronic and magnetoelectronic devices.[143] Thus, these graphene molecules, carbon nanotubes, and fullerenes are composed of a kind of useful carbon-based material for various applications.

8. Acknowledgments

The EU financial support through the NAIMO integrated project, No. NMP4-CT-2004-500355, is gratefully acknowledged. The authors also acknowledge the financial support from the Deutsche Forschungsgemeinschaft (Schwerpunkt organische Feldeffekttransistoren).

9. References

(1) (a) Clar, E. *Polycyclic Hydrocarbons*; Academic Press: New York, 1964; Vol. I/II. (b) Clar, E. *The Aromatic Sextet*; Wiley-VCH: London, 1972. (c) Scholl, R.; Seer, C.; Weitzenbök, R. *Chem. Ber.* **1910**, *43*, 2202. (d) Scholl, R.; Seer, C. *Liebigs Ann. Chem.* **1912**, *394*, 111. (e) Scholl, R.; Seer, C. *Chem. Ber.* **1922**, *55*, 330. (f) Clar, E.; Stewart, D. G. *J. Am. Chem. Soc.* **1953**, *75*, 2667. (g) Clar, E.; Schmidt, W. *Tetrahedron* **1979**, *35*, 2673.

(2) (a) Goh, S. H.; Harvey, R. G. *J. Am. Chem. Soc.* **1973**, *95*, 242. (b) Harvey, R. G.; Zhang, J.-T.; Luna, E.; Pataki, J. *J. Org. Chem.* **1998**, *63*, 6405.

(3) (a) Harvey, R. G. *Polycyclic Aromatic Hydrocarbons*; Wiley-VCH: New York, 1997. (b) *Carbon Rich Compounds I/II*; Topics in Current Chemistry; Springer: Berlin, 1998, Vol. 196; 1999, Vol. 201.

(4) (a) De Proft, F.; Geerlings, P. *Chem. Rev.* **2001**, *101*, 1451. (b) Mitchell, R. H. *Chem. Rev.* **2001**, *101*, 1301. (c) Slayden, S. W.; Liebman, J. F. *Chem. Rev.* **2001**, *101*, 1541.

(5) Goddard, R.; Haenel, M. W.; Herndon, W. C.; Krueger, C.; Zander, M. *J. Am. Chem. Soc.* **1995**, *117*, 30.

(6) See 2000 Nobel Prize lectures: (a) Shirakawa, H. *Angew. Chem.* **2001**, *113*, 2642; *Angew. Chem., Int. Ed.* **2001**, *40*, 2574. (b) MacDiarmid, A. G. *Angew. Chem.* **2001**, *113*, 2649; *Angew. Chem., Int. Ed.* **2001**, *40*, 2581. (c) Heeger, A. J. *Angew. Chem.* **2001**, *113*, 2660; *Angew. Chem., Int. Ed.* **2001**, *40*, 2591.

(7) (a) *Handbook of Conducting Polymers*, 2nd ed.; Skotheim, T. A., Elsenbaumer, R. L., Reynolds, J. R., Eds.; Marcel Dekker, Inc.: New York, 1998. (b) *Semiconducting Polymers: Chemistry, Physics, and Engineering*; Hadziioannou, G., van Hutten, P. F., Eds.; Wiley-VCH: Weinheim, 2000.

(8) (a) Wang, Z. H.; Li, C.; Scherr, E. M.; MacDiarmid, A. G.; Epstein, A. J. *Phys. Rev. Lett.* **1991**, *66*, 1745. (b) Aleshin, A.; Kiebooms, R.; Menon, R.; Wudl, F.; Heeger, A. J. *Phys. Rev. B* **1997**, *56*, 3659. (c) Heeger, A. J. *J. Phys. Chem. B* **2001**, *105*, 8475. (d) Sirringhaus, H.; Brown, P. J.; Friend, R. H.; Nielsen, M. M.; Bechgaard, K.; Langeveld-Voss, B. M. W.; Spiering, A. J. H.; Janssen, R. A. J.; Meijer, E. W.; Herwig, P.; de Leeuw, D. M. *Nature* **1999**, *401*, 685.

(9) van de Craats, A. M.; Warman, J. M.; De Hass, M. P.; Adam, D.; Simmerer, J.; Haarer, D.; Schuhmacher, P. *Adv. Mater.* **1996**, *8*, 823.

(10) Sundar, V. C.; Zaumseil, J.; Podzorov, V.; Menard, E.; Willett, R. L.; Someya, T.; Gershenson, M. E.; Rogers, J. A. *Science* **2004**, *303*, 1644.

(11) O'Neill, M.; Kelly, S. M. *Adv. Mater.* **2003**, *15*, 1135.

(12) *Electronic Materials: The Oligomer Approach*; Müllen, K., Wegner, G., Eds.; Wiley-VCH: Weinheim, 1998.

(13) Sirringhaus. H. *Adv. Mater.* **2005**, *17*, 2411.

(14) Martin, R. E.; Diederich, F. *Angew. Chem., Int. Ed.* **1999**, *38*, 1350.

(15) (a) Sage, I. C. In *Handbook of Liquid Crystals*; Demus, D., Goodby, J., Gray, G. W., Spiess, H. W., Vill, V., Eds.; Wiley-VCH: Weinheim, 1998; Vol. 1, p 731. (b) Watson, M. D.; Fechtenkötter, A.; Müllen, K. *Chem. Rev.* **2001**, *101*, 1267. (c) Simpson, C. D.; Wu, J.; Watson, M. D.; Müllen, K. *J. Mater. Chem.* **2004**, *14*, 494. (d) Bushby, R. J.; Lozman, O. R. *Curr. Opin. Solid State Mater. Sci.* **2002**, *6*, 569.

(16) Pisula, W.; Tomović, Ž.; Simpson, C. D.; Kastler, M.; Pakula, T.; Müllen, K. *Chem. Mater.* **2005**, *17*, 4296.

(17) Levelut, A. M.; Hardouin, F.; Gasparoux, H.; Destrade, C.; Tinh, N. H. *J. Physique* **1981**, 147.

(18) (a) Gearba, R.; Bondar, A. I.; Goderis, B.; Bras, W.; Ivanov, D. A. *Chem. Mater.* **2005**, *17*, 2825. (b) Holst, H. C.; Pakula, T.; Meier, H. *Tetrahedron* **2004**, *60*, 6765.

(19) (a) Fischbach, I.; Pakula, T.; Minkin, P.; Fechtenkötter, A.; Müllen, K.; Spiess, H. W.; Saalwachter, K. *J. Phys. Chem. B* **2002**, *106*, 6408. (b) Fischbach, I.; Ebert, F.; Spiess, H. W.; Schnell, I. *Chem. Phys. Chem.* **2004**, *5*, 895.

(20) (a) Beeson, J. C.; Fitzgerald, L. J.; Gallucci, J. C.; Gerkin, R. E.; Rademacher, J. T.; Czarnik, A. W. *J. Am. Chem. Soc.* **1994**, *116*, 4621. (b) Gearba, R. I.; Lehmann, M.; Levin, J.; Ivanov, D. A.; Koch, M. H. J.; Barbera, J.; Debije, M. G.; Piris, J.; Geerts, Y. H. *Adv. Mater.* **2003**, *15*, 1614.

(21) Liu, C. Y.; Bard, A. J. *Nature* **2002**, *418*, 162.

(22) (a) van de Craats, A. M.; Warman, J. M.; Müllen, K.; Geerts, Y.; Brand, J. *Adv. Mater.* **1998**, *10*, 36. (b) van de Craats, A. M.; Warman, J. M.; Fechtenkötter, A.; Brand, J. D.; Harbison, M. A.; Müllen, K. *Adv. Mater.* **1999**, *11*, 1469.

(23) Warman, J. M.; Piris, J.; Pisula, W.; Kastler, M.; Wasserfallen, D.; Müllen, K. *J. Am. Chem. Soc.* **2005**, *127*, 14257.

(24) (a) Clar, E.; Ironside, C. T. *Proc. Chem. Soc.* **1958**, 150. (b) Clar, E.; Ironside, C. T.; Zander, M. *J. Chem. Soc.* **1959**, 142.

(25) Halleux, A.; Martin, R. H.; King, G. S. D. *Helv. Chim. Acta* **1958**, *129*, 1177.

(26) Hendel, W.; Khan, Z. H.; Schmidt, W. *Tetrahedron* **1986**, *42*, 1127.

(27) (a) Stabel, A.; Herwig, P.; Müllen, K.; Rabe, J. P. *Angew. Chem.* **1995**, *107*, 1768; *Angew. Chem., Int. Ed. Engl.* **1995**, *34*, 1609. (b) Müller, M.; Kübel, C.; Müllen, K. *Chem.—Eur. J.* **1998**, *4*, 2099.

(28) (a) Moore, J. S. *Acc. Chem. Res.* **1997**, *30*, 402. (b) Höger, S. *J. Polym. Sci., Part A: Polym. Chem.* **1999**, *37*, 2685. (c) Haley, M. M. *Top. Curr. Chem.* **1999**, *201*, 81. (d) Bong, D. T.; Clark, T. D.; Granja, J. R.; Ghadiri, M. R. *Angew. Chem., Int. Ed.* **2001**, *40*, 988.

(29) Kastler, M.; Pisula, W.; Wasserfallen, D.; Pakula, T.; Müllen, K. *J. Am. Chem. Soc.* **2005**, *127*, 4268.

(30) (a) Salaneck, W. R.; Seki, K.; Kahn, A.; Pireaux, J.-J. *Conjugated Polymer and Molecular Interfaces: Science and Technology for Photonic and Optoelectronic Applications*; Marcel Dekker: New York, 2001. (b) Kahn, A.; Koch, N.; Gao, W. Y. *J. Polym. Sci., B* **2003**, *4*, 2529.

(31) Rabe, J. P.; Buchholz, S. *Science* **1991**, *253*, 424.

(32) (a) Haughman, H.; Zakhidov, A. A.; de Heer, W. A. *Science* **2002**, *297*, 787. (b) Subramoney, S. *Adv. Mater.* **1998**, *10*, 1157. (c) Dai, H. *Surf. Sci.* **2002**, *500*, 218. (d) Fan, S.; Chapline, M. G.; Franklin, N. R.; Tombler, T. W.; Cassell, A. M.; Dai, H. *Science* **1999**, *283*, 512. (e) Chen, P.; Wu, X.; Lin, J.; Tan, K. L. *Science* **1999**, *285*, 91. (f) Dai, H.; Wong, E. W.; Lieber, C. M. *Science* **1996**, *272*, 523. (g) Kong, J.; Franklin, N. R.; Zhou, C.; Chapline, M. G.; Peng, S.; Cho, K.; Dai, H. *Science* **2000**, *287*, 622. (h) Liu, C.; Fan, Y. Y.; Liu, M.; Cong, H. T.; Cheng, H. M.; Dresselhaus, M. S. *Science* **1999**, *286*, 1127.

(33) Balaban, A. T.; Nenitzescu C. D. In *Friedel-Crafts and Related Reactions*; Olah G. A., Ed; Interscience: New York, 1964; Vol. 2, Part 2, p 979.

(34) Kovacic, P.; Jones, M. B. *Chem. Rev.* **1987**, *87*, 357.

(35) Hyatt, J. A. *Org. Prep. Proced. Int.* **1991**, *23*, 460.

(36) Kübel, C.; Eckhardt, K.; Enkelmann, V.; Wegner, G.; Müllen, K. *J. Mater. Chem.* **2000**, *10*, 879.

(37) Herwig, P.; Kayser, C. W.; Müllen, K.; Spiess, H. W. *Adv. Mater.* **1996**, *8*, 510.

(38) Fechtenkötter, A.; Saalwächter, K.; Harbison, M. A.; Müllen, K.; Spiess, H. W. *Angew. Chem.* **1999**, *111*, 3224; *Angew. Chem., Int. Ed.* **1999**, *38*, 3039.

(39) (a) Ito, S.; Wehmeier, M.; Brand, J. D.; Kübel, C.; Epsch, R.; Rabe, J. P.; Müllen, K. *Chem.—Eur. J.* **2000**, *6*, 4327. (b) Fechtenkötter, A.; Tchebotareva, N.; Watson, M. D.; Müllen, K. *Tetrahedron* **2001**, *57*, 3769.

(40) Weiss, K.; Beernink, G.; Dötz, F.; Birkner, A.; Müllen, K.; Wöll, C. H. *Angew. Chem.* **1999**, *111*, 3974; *Angew. Chem., Int. Ed.* **1999**, *38*, 3748.

(41) (a) Lambert, C.; Nöll, G. *Angew. Chem.* **1998**, *110*, 2239; *Angew. Chem., Int. Ed.* **1998**, *37*, 2107. (b) Lambert, C.; Nöll, G. *Chem.—Eur. J.* **2002**, *8*, 3467.

(42) (a) Wu, J.; Gherghel, L.; Watson, M. D.; Li, J.; Wang, Z.; Simpson, C. D.; Kolb, U.; Müllen, K. *Macromolecules* **2003**, *36*, 7082. (b) Feng, X.; Wu, J.; Enkelmann, V.; Müllen, K. *Org. Lett.* **2006**, *8*, 1145.

(43) Wu, J.; Baumgarten, M.; Debije, M. G.; Warman, J. M.; Müllen, K. *Angew. Chem.* **2004**, *116*, 5445; *Angew. Chem., Int. Ed.* **2004**, *43*, 5331.

(44) (a) Rempala, P.; Kroulik, J.; King, J. B. T. *Am. Chem. Soc.* **2004**, *126*, 15002. (b) Stefano, M. D.; Negri, F.; Carbone, P.; Müllen, K. *Chem. Phys.* **2005**, *314*, 85.

(45) (a) Wu, J.; Watson, M. D.; Müllen, K. *Angew. Chem.* **2003**, *115*, 5487; *Angew. Chem., Int. Ed.* **2003**, *42*, 5329. (b) Wu, J.; Watson, M. D.; Zhang, L.; Wang, Z.; Müllen, K. *J. Am. Chem. Soc.* **2004**, *126*, 177.

(46) Wu, J.; Li, J.; Kolb, U.; Müllen, K. *Chem. Commun.* **2006**, 48.

(47) Lee, M.; Kim, J.; Peleshanko, S.; Larson, K.; Yoo, Y.; Vaknin, D.; Markutsya, S.; Tsukruk, V. V. *J. Am. Chem. Soc.* **2002**, *124*, 9121.

(48) Wang, Z.; Dötz, F.; Enkelmann, V.; Müllen, K. *Angew. Chem.* **2005**, *117*, 1273; *Angew. Chem., Int. Ed.* **2005**, *44*, 1247.

(49) Xiao, S.; Myers, M.; Miao, Q.; Sanaur, S.; Pang, K.; Steigerwald, M. L.; Nuckolls, C. *Angew. Chem., Int. Ed.* **2005**, *44*, 7390.

(50) Clar, E.; Stephen, J. F. *Tetrahedron* **1965**, *21*, 467.

(51) Debije, M. G.; Piris, J.; de Haas, M. P.; Warman, J. M.; Tomović, Ž.; Simpson, C. D.; Watson, M. D.; Müllen, K. *J. Am. Chem. Soc.* **2004**, *126*, 4641.

(52) Wu, J.; Tomović, Ž; Enkelmann, V.; Müllen, K. *J. Org. Chem.* **2004**, *69*, 5179.

(53) Tomović, Ž.; Watson, M. D.; Müllen, K. *Angew. Chem.* **2004**, *116*, 733; *Angew. Chem., Int. Ed.* **2004**, *43*, 755.

(54) Simpson, C. D. Ph.D. Thesis, University of Mainz, 2003.

(55) Simpson, C. D.; Brand, J. D.; Berresheim, A. J.; Przybilla, L.; Räder, H. J.; Müllen, K. *Chem.—Eur. J.* **2000**, *8*, 1424.

(56) (a) Scott, L. T.; Boorum, M. M.; McMahon, B.; Hagen, S.; Mack, J.; Blank, J.; Wegner, H.; de Meijere, A. *Science* **2002**, *295*, 1500. (b) Boorum, M. M.; Vasil'ev, Y. V.; Drewello, T.; Scott, L. T. *Science* **2001**, *294*, 828.

(57) Simpson, C. D.; Mattersteig, G.; Martin, K.; Gherghel, L.; Bauer, R. E.; Räder, H. J.; Müllen, K. *J. Am. Chem. Soc.* **2004**, *126*, 3139.

(58) Megahead, S.; Scosati, B. *J. Power Sources* **1994**, *51*, 79.

(59) (a) Iyer, V. S.; Yoshimura, K.; Enkelmann, V.; Epsch, R.; Rabe, J. P.; Müllen, K. *Angew. Chem.* **1998**, *110*, 2843; *Angew. Chem., Int. Ed.* **1998**, *37*, 2696. (b) Müller, M.; Iyer, V. S.; Kübel, C.; Enkelmann, V.; Müllen, K. *Angew. Chem.* **1997**, *109*, 1679; *Angew. Chem., Int. Ed.* **1997**, *36*, 1607.

(60) (a) Iyer, V. S.; Wehmeier, M.; Brand, J. D.; Keegstra, M. A.; Müllen, K. *Angew. Chem.* **1997**, *109*, 1676; *Angew. Chem., Int. Ed.* **1997**, *36*, 1603. (b) Wasserfallen, D.; Kastler, M.; Pisula, W.; Hofer, W. A.; Fogel, Y.; Wang, Z.; Müllen, K. *J. Am. Chem. Soc.* **2006**, *128*, 1334.

(61) Wu, J.; Watson, M. D.; Tchebotareva, N.; Wang, Z.; Müllen, K. *J. Org. Chem.* **2004**, *69*, 8194.

(62) Stein, S. E.; Brown, R. L. *J. Am. Chem. Soc.* **1987**, *109*, 3721.

(63) Dötz, F.; Brand, J. D.; Ito, S.; Gherghel, L.; Müllen, K. *J. Am. Chem. Soc.* **2000**, *122*, 7707.

(64) Clar, E.; Boggiano, B. *J. Chem. Soc.* **1957**, 2683.

(65) (a) Wang, Z.; Tomović, Ž.; Kastler, M.; Pretsch, R.; Negri, F.; Enkelmann, V.; Müllen, K. *J. Am. Chem. Soc.* **2004**, *126*, 7794. (b) Kastler, M.; Schmidt, J.; Pisula, W.; Müllen, K. *J. Am. Chem. Soc.* **2006**, *128*, 9526.

(66) Wu, J.; Fechtenkötter, A.; Gauss, J.; Watson, M. D.; Kastler, M.; Fechtenkötter, C.; Wagner, M.; Müllen, K. *J. Am. Chem. Soc.* **2004**, *126*, 11311.

(67) (a) Fleming, A. J.; Coleman, J. N.; Dalton, A. B.; Fechtenkötter, A.; Watson, M. D.; Müllen, K.; Byrne, H. J.; Blau, W. J. *J. Phys. Chem. B* **2003**, *107*, 37. (b) Bayer, A.; Hübner, J.; Kopitzke, J.; Oestreich, M.; Rühle, W.; Wendorff, J. H. *J. Phys. Chem. B* **2001**, *105*, 4596. (c) Marguet, S.; Markovitsi, D.; Millié, P.; Sigal, H.; Kumar, S. *J. Phys. Chem. B* **1998**, *102*, 4697.

(68) Wu, J.; Qu, J.; Tchebotareva, N.; Müllen, K. *Tetrahedron Lett.* **2005**, *46*, 1565.

(69) Draper, S. M.; Gregg, D. J.; Madathil, R. *J. Am. Chem. Soc.* **2002**, *124*, 3486.

(70) Draper, M. S.; Gregg, D. J.; Schofield, E. R.; Browne, W. R.; Duati, M.; Vos, J. G.; Passaniti, P. *J. Am. Chem. Soc.* **2004**, *126*, 8694.

(71) (a) Chávez, I.; Cisternas, A.; Otero, M.; Román, E. *Z. Naturforsch.* **1990**, *45b*, 658. (b) Seiders, T. J.; Baldridge, K. K.; O'Connor, J. M.; Siegel, J. S. *J. Am. Chem. Soc.* **1997**, *119*, 4781. (c) Vecchi, P. A.; Alvarez, C. M.; Ellern, A.; Angelici, R. J.; Sygula, A.; Sygula, R.; Rabideau, P. W. *Angew. Chem.* **2004**, *116*, 4597; *Angew. Chem., Int. Ed.* **2004**, *43*, 4497.

(72) Lukas, N. T.; Wu, J.; Enkelmann, V.; Müllen, K.; Willis, A. C. Submitted.

(73) (a) *Cyclophanes*; Dunitz, J. D., Hafner, K., Ito, S., Lehn, J. M., Raymond, K. N., Rees, C. W., Thiem, J., Vögtle, F., Eds.; Springer-Verlag: Berlin, 1994. (b) *Modern Cyclophane Chemistry*; Hopf, H., Gleiter, R., Eds.; Wiley-VCH: Weinheim, 2004.

(74) Watson, M. D.; Jäckel, F.; Severin, N.; Rabe, J. P.; Müllen, K. *J. Am. Chem. Soc.* **2004**, *126*, 1402.

(75) Donohoe, T. J.; Garg, R.; Stevenson, C. A. *Tetrahedron: Asymmetry* **1996**, *7*, 317.

(76) Watson, M. D.; Debije, M. G.; Warman, J. M.; Müllen, K. *J. Am. Chem. Soc.* **2004**, *126*, 766.

(77) (a) Herogues, V.; Gnanou, Y.; Fontanille, M. *Macromolecules* **1997**, *30*, 4791. (b) Saito, R.; Fujita, A.; Ichimura, A.; Ishizu, K. *J. Polym. Sci. Polym. Chem.* **2000**, *38*, 2091; Tauer, K.; Khrenov, V. *Macromol. Symp.* **2002**, *179*, 27.

(78) Bo, Z.; Rabe, J. P.; Schlüter, A. D. *Angew. Chem.* **1999**, *111*, 2540; *Angew. Chem., Int. Ed.* **1999**, *38*, 2370.

(79) Hoeben, F. J. M.; Jonkheijm, P.; Meijer, E. W.; Schenning, A. P. H. J. *Chem. Rev.* **2005**, *105*, 1491.

(80) Tchebotareva, N. Ph.D. Thesis, University of Mainz, 2003.

(81) (a) Hill, J. P.; Jin, W.; Kosaka, A.; Fukushima, T.; Ichihara, H.; Shimomura, T.; Ito, K.; Hashizume, T.; Ishii, N.; Aida, T. *Science* **2004**, *304*, 1481. (b) Jin, W.; Fukushima, T.; Niki, M.; Kosaka, A.; Ishii, N.; Aida, T. *Proc. Natl. Acad. Sci. U.S.A.* **2005**, *102*, 10801. (c) Jin, W.; Fukushima, T.; Kosaka, A.; Niki, M.; Ishii, N.; Aida, T. *J. Am. Chem. Soc.* **2005**, *127*, 8284. (d) Motoyanagi, J.; Fukushima, T.; Ishii, N.; Aida, T. *J. Am. Chem. Soc.* **2006**, *128*, 4220.

(82) Brand, J. D.; Kübel, C.; Ito, S.; Müllen, K. *Chem. Mater.* **2000**, *12*, 1683.

(83) Spraul, B. K.; Suresh, S.; Glaser, S.; Perahia, D.; Ballato, J.; Smith, D. W., Jr. *J. Am. Chem. Soc.* **2004**, *126*, 12772.

(84) Levelut, A. M.; Hardouin, F.; Gasparoux, H.; Destrade, C.; Tinh, N. H. *J. Phys.* **1981**, 147.

(85) Pisula, W.; Tomović, Ž.; Simpson, C. D.; Kastler, M.; Pakula, T.; Müllen, K. *Chem. Mater.* **2005**, *17*, 4296.

(86) Boden, N.; Bushby, R. J.; Clements, J.; Movaghar, B.; Donovan, K. J.; Kreouzis, T. *Phys. Rev. B* **1995**, *52*, 13274.

(87) (a) Fischbach, I.; Pakula, T.; Minkin, P.; Fechtenkotter, A.; Müllen, K.; Spiess, H. W.; Saalwachter, K. *J. Phys. Chem. B* **2002**, *106*, 6408. (b) Fischbach, I.; Ebert, F.; Spiess, H. W.; Schnell, I. *ChemPhysChem* **2004**, *5*, 895.

(88) Brown, S. P.; Schnell, I.; Brand, J. D.; Müllen, K.; Spiess, H. W. *J. Am. Chem. Soc.* **1999**, *121*, 6712.

(89) (a) Brunsveld, L.; Folmer, B. J. B.; Meijer, E. W.; Sijbesma, R. P. *Chem. Rev.* **2001**, *101*, 4071. (b) Ciferri, A. *Macromol. Rapid Commun.* **2002**, *23*, 511.

(90) (a) Wasserfallen, D.; Fischbach, I.; Tchebotareva, N.; Kastler, M.; Pisula, W.; Jäckel, F.; Watson, M. D.; Schnell, I.; Rabe, J. P.; Spiess, H. W.; Müllen, K. *Adv. Funct. Mater.* **2005**, *15*, 1585. (b) Samori, P.; Yin, X. M.; Tchebotareva, N.; Wang, Z. H.; Pakula, T.; Jackel, F.; Watson, M. D.; Venturini, A.; Müllen, K.; Rabe, J. P. *J. Am. Chem. Soc.* **2004**, *126*, 3567.

(91) van de Craats, A. M.; Siebbeles, L. D. A.; Bleyl, I.; Haarer, D.; Berlin, Y. A.; Zharikov, A. A.; Warman, J. M. *J. Phys. Chem. B* **1998**, *102*, 9625.

(92) Glusen, B.; Heitz, W.; Kettner, A.; Wendorff, J. H. *Liq. Cryst.* **1996**, *20*, 627.

(93) Banach, M. J.; Friend, R. H.; Sirringhaus, H. *Macromolecules* **2004**, *37*, 6079.

(94) Kastler, M.; Pisula, W.; Wasserfallen, D.; Pakula, T.; Müllen, K. *J. Am. Chem. Soc.* **2005**, *127*, 4268.

(95) Tracz, A.; Pakula, T.; Jeszka, J. K. *Mater. Sci. (Poland)* **2004**, *22*, 415.

(96) (a) Tracz, A.; Jeszka, J. K.; Kryszewski, M.; Shafee, E. E. *Mater. Sci. (Poland)* **1988**, *14*, 181. (b) Tang, C.; Tracz, A.; Kruk, M.; Zhang, R.; Smilgies, D.-M.; Matyjaszewski, K.; Kowalewski, T. *J. Am. Chem. Soc.* **2005**, *127*, 6918.

(97) Tracz, A.; Jeszka, J. K.; Watson, M. D.; Pisula, W.; Müllen, K.; Pakula, T. *J. Am. Chem. Soc.* **2003**, *125*, 1682.

(98) Pisula, W.; Menon, A.; Stepputat, M.; Lieberwirth, I.; Kolb, U.; Tracz, A.; Sirringhaus, H.; Pakula, T.; Müllen, K. *Adv. Mater.* **2005**, *17*, 684.

(99) (a) Breiby, D. W.; Bunk, O.; Pisula, W.; Sølling, T. I.; Tracz, A.; Pakula, T.; Müllen, K.; Nielsen, M. M. *J. Am. Chem. Soc.* **2005**,

SAMSUNG EX. 1012 - 29/30

127, 11288. (b) Breiby, D. W.; Hansteen, F.; Pisula, W.; Bunk, O.; Kolb, U.; Andreasen, J. W.; Müllen, K.; Nielsen, M. M. *J. Phys. Chem. B* **2005**, *109*, 22319.
(100) Piris, J.; Debije, M. G.; Stutzmann, N.; Laursen, B. W.; Pisula, W.; Watson, M. D.; Bjornholm, T.; Müllen, K.; Warman, J. M. *Adv. Funct. Mater.* **2004**, *14*, 1053.
(101) Piris, J.; Pisula, W.; Tracz, A.; Pakula, T.; Müllen, K.; Warman, J. *Liq. Cryst.* **2004**, *31*, 993.
(102) Piris, J.; Pisula, W.; Warman, J. M. *Synth. Met.* **2004**, *147*, 85.
(103) Pisula, W.; Tomović, Ž.; Stepputat, M.; Kolb, U.; Pakula, T.; Müllen, K. *Chem. Mater.* **2005**, *17*, 2641.
(104) Shklyarevskiy, I. O.; Jonkheijm, P.; Stutzmann, N.; Wasserberg, D.; Wondergem, H. J.; Christianen, P. C. M.; Schenning, A. P. H. J.; de Leeuw, D. M.; Tomović, Ž.; Wu, J.; Müllen, K.; Maan, J. C. *J. Am. Chem. Soc.* **2005**, *127*, 16233.
(105) Zimmermann, S.; Wendorff, J. H.; Wedder, C. *Chem. Mater.* **2002**, *14*, 2218.
(106) van de Craats, A. M.; Stutzmann, N.; Bunk, O.; Nielsen, M. M.; Watson, M.; Müllen, K.; Chanzy, H. D.; Sirringhaus, H.; Friend, R. H. *Adv. Mater.* **2003**, *15*, 495.
(107) (a) Piris, J.; Debije, M. G.; Stutzmann, N.; van de Craats, A. M.; Watson, M. D.; Müllen, K.; Warman, J. M. *Adv. Mater.* **2003**, *15*, 1736. (b) Bunk, O.; Nielsen, M. M.; Solling, T. I.; van de Craats, A. M.; Stutzmann, N. *J. Am. Chem. Soc.* **2003**, *125*, 2252.
(108) (a) Mindyuk, O. Y.; Heiney, P. A. *Adv. Mater.* **1999**, *11*, 341. (b) Armstrong, N. R. *J. Porphyrins Phthalocyanines* **2000**, *4*, 414.
(109) Reitzel, N.; Hassenkam, T.; Balashev, K.; Jensen, T. R.; Howes, P. B.; Kjaer, K.; Fechtenkötter, A.; Tchebotareva, N.; Ito, S.; Müllen, K.; Bjϕrnholm, T. *Chem.—Eur. J.* **2001**, *7*, 4894.
(110) Laursen, B. W.; Norgaard, K.; Reitzel, N.; Simonsen, J. B.; Nielsen, C. B.; Als-Nielsen, J.; Bjornholm, T.; Solling, T. I.; Nielsen, M. M.; Bunk, O.; Kjaer, K.; Tchebotareva, N.; Watson, M. D.; Müllen, K.; Piris, J. *Langmuir* **2004**, *20*, 4139.
(111) (a) Kubowicz, S.; Thunemann, A. F.; Geue, T. M.; Pietsch, U.; Watson, M. D.; Tchebotareva, N.; Müllen, K. *Langmuir* **2003**, *19*, 10997. (b) Kubowicz, S.; Pietsch, U.; Watson, M. D.; Tchebotareva, N.; Müllen, K.; Thunemann, A. F. *Langmuir* **2003**, *19*, 5036. (c) Thüneman, A. F.; Ruppelt, D.; Ito, S.; Müllen, K. *J. Mater. Chem.* **1999**, *9*, 1055.
(112) Pisula, W.; Kastler, M.; Wasserfallen, D.; Mondeshki, M.; Piris, J.; Schnell, I.; Müllen, K. *Chem. Mater.* **2006**, *18*, 3634.
(113) (a) Kastler, M.; Pisula, W.; Laquai, F.; Kumar, A.; Davis, R.; Baluschev, S.; Garcia-Gutiérrez, M. C.; Wasserfallen, D.; Butt, H.-J.; Riekel, C.; Wegner, G.; Müllen, K. *Adv. Mater.* **2006**, *18*, 2255. (b) Pisula, W.; Kastler, M.; Wasserfallen, D.; Robertson, J. W. F.; Nolde, F.; Kohl, C.; Müllen, K. *Angew. Chem., Int. Ed.* **2006**, *45*, 819.
(114) Lovinger, A. J.; Gryte, C. C. *Macromolecules* **1976**, *9*, 247.
(115) (a) Pisula, W.; Kastler, M.; Wasserfallen, D.; Pakula, T.; Müllen, K. *J. Am. Chem. Soc.* **2004**, *126*, 8074. (b) Pisula, W.; Kastler, M.; Wasserfallen, D.; Davies, R. J.; Garcia-Gutierrez, M.-C.; Müllen, K. *J. Am. Chem. Soc.* **2006**, *128*, 14424.
(116) Hatsusaka, K.; Ohta, K.; Yamamoto, I.; Shirai, H. *J. Mater. Chem.* **2001**, *11*, 423.
(117) (a) Pisula, W.; Tomović, Ž.; El Hamaoui, B.; Watson, M. D.; Pakula, T.; Müllen, K. *Adv. Funct. Mater.* **2005**, *15*, 893. (b) Pisula, W.; Kastler, M.; El Hamaoui, B.; García-Gutiérrez, M.-C.; Davies, R. J.; Riekel, C.; Müllen, K. Submitted.
(118) Liu, C. Y.; Fechtenkötter, A.; Watson, M. D.; Müllen, K.; Bard, A. J. *Chem. Mater.* **2003**, *15*, 124.
(119) Schmidt-Mende, L.; Fechtenkötter, A.; Müllen, K.; Moons, E.; Friend, R. H.; MacKenzie, J. D. *Science* **2001**, *293*, 1119.
(120) (a) Keil, M.; Samorí, P.; dos Santos, D. A.; Kugler, T.; Stafström, S.; Brand, J. D.; Müllen, K.; Brédas, J. L.; Rabe, J. P.; Salaneck, W. R. *J. Phys. Chem. B* **2000**, *104*, 3967. (b) Ruffieux, P.; Gröning, O.; Bielmann, M.; Simpson, C.; Müllen, K.; Schlapbach, L.; Gröning, P. *Phys. Rev. B* **2002**, *66*, 073409.
(121) Qiu, X.; Wang, C.; Zeng, Q.; Xu, B.; Yin, S.; Wang, H.; Xu, S.; Bai, C. *J. Am. Chem. Soc.* **2000**, *122*, 5550.
(122) Piot, L.; Marchenko, A.; Fichou, D.; Wu, J.; Müllen, K. *J. Am. Chem. Soc.* **2005**, *127*, 16245.
(123) Samorí, P.; Fechtenkötter, A.; Jackel, F.; Böhme, T.; Müllen, K.; Rabe, J. P. *J. Am. Chem. Soc.* **2001**, *123*, 11462.
(124) Ito, S.; Herwig, P. T.; Böhme, T.; Rabe, J. P.; Rettig, W.; Müllen, K. *J. Am. Chem. Soc.* **2000**, *122*, 7698.
(125) Samorí, P.; Severin, N.; Simpson, C. D.; Müllen, K.; Rabe, J. P. *J. Am. Chem. Soc.* **2002**, *124*, 9454.
(126) Tchebotareva, N.; Yin, X. M.; Watson, M. D.; Samori, P.; Rabe, J. P.; Müllen, K. *J. Am. Chem. Soc.* **2003**, *125*, 9734.
(127) Jäckel, F.; Wang, Z.; Watson, M. D.; Müllen, K.; Rabe, J. P. *Chem. Phys. Lett.* **2004**, *387*, 372.
(128) Jäckel, F.; Watson, M. D.; Müllen, K.; Rabe, J. P. *Phys. Rev. Lett.* **2004**, *92*, 188301-1.
(129) (a) Li, Z.; Jaroniec, M.; Lee, Y. J.; Radovic, L. R. *Chem. Commun.* **2002**, 1346. (b) Yoon, S. B.; Chai, G. S.; Kang, S. K.; Yu, J.-S.; Gierszal, K. P.; Jaroniec, M. *J. Am. Chem. Soc.* **2005**, *127*, 4188.
(130) Steinhart, M.; Zimmermann, S.; Goring, P.; Schaper, A. K.; Gosele, U.; Weder, C.; Wendorff, J. H. *Nano Lett.* **2005**, *5*, 429.
(131) Gherghel, L.; Kübel, C.; Lieser, G.; Räder, H. J.; Müllen, K. *J. Am. Chem. Soc.* **2002**, *124*, 13130.
(132) (a) Jian, K.; Shim, H.; Schwartzman, A.; Crawford, G. P.; Hurt, R. H. *Adv. Mater.* **2003**, *15*, 164. (b) Zhi, L.; Wu, J.; Li, J.; Kolb, U.; Mülen, K. *Angew. Chem.* **2005**, *117*, 2158; *Angew. Chem., Int. Ed.* **2005**, *44*, 2120.
(133) (a) Steinhart, M.; Wendorff, J. H.; Greiner, A.; Wehrspohn, R. B.; Nielsch, K.; Schilling, J.; Choi, J.; Gösele, U. *Science* **2002**, *296*, 1997. (b) Steinhart, M.; Wehrspohn, R. B.; Gösele, U.; Wendorff, J. H. *Angew. Chem.* **2004**, *116*, 1356; *Angew. Chem., Int. Ed.* **2004**, *43*, 1334.
(134) Zhi, L.; Gorelik, T.; Wu, J.; Kolb, U.; Müllen, K. *J. Am. Chem. Soc.* **2005**, *127*, 12792.
(135) Zhi, L.; Wu, J.; Li, J.; Stepputat, M.; Kolb, U.; Müllen, K. *Adv. Mater.* **2005**, *17*, 1492.
(136) (a) Dosa, P. I.; Erben, C.; Iyer, V. S.; Vollhardt, K. P.; Wasser, I. M. *J. Am. Chem. Soc.* **1999**, *121*, 10430. (b) Boese, R.; Matzger, A. J.; Vollhardt, K. P C. *J. Am. Chem. Soc.* **1997**, *119*, 2052. (c) Dosa, P. I.; Schleifenbaum, A.; Vollhardt, K. P. C. *Org. Lett.* **2001**, *3*, 1017. (d) Bunz. U. H. F. *J. Organomet. Chem.* **2003**, *683*, 269. (e) Laskoski, M.; Steffen, W.; Morton, J. G. M.; Smith, M. D.; Bunz, U. H. F. *J. Am. Chem. Soc.* **2002**, *124*, 13814. (f) Scholz, S.; Leech, P. J.; Englert, B. C.; Sommer, W.; Weck, M.; Bunz, U. H. F. *Adv. Mater.* **2005**, *17*, 1052.
(137) Iyer, V. S.; Vollhardt, K. P. C.; Wilhelm, R. *Angew. Chem.* **2003**, *115*, 4515; *Angew. Chem., Int. Ed.* **2003**, *42*, 4379.
(138) Wu, J.; El Hamaoui, B.; Li, J.; Zhi, L.; Kolb, U.; Müllen, K. *Small* **2005**, *1*, 210.
(139) El Hamaoui, B.; Wu, J.; Zhi, L.; Müllen, K. *Adv. Mater.* **2005**, *17*, 2957.
(140) Megahead, S.; Scrosati, B. *J. Power Sources* **1994**, *51*, 79.
(141) (a) Renouard, T.; Gherghel, L.; Wachtler, M.; Bonino, F.; Scrosati, B.; Nuffer, R.; Mathis, C.; Müllen, K. *J. Power Sources* **2005**, *139*, 242. (b) Bonino, F.; Brutti, S.; Reale, P.; Scrosati, B.; Gherghel, L.; Wu, J.; Müllen, K. *Adv. Mater.* **2005**, *17*, 743.
(142) Niyogi, S.; Bekyarova, E.; Itkis, M. E.; McWilliams, J. L.; Hamon, M. A.; Haddon, R. C. *J. Am. Chem. Soc.* **2006**, *128*, 7720.
(143) (a) Novoselov, K. S.; Geim, A. K.; Morozov, S. V.; Jiang, D.; Zhang, Y.; Dubonos, S. V.; Grigorieva, I. V.; Firsov, A. A. *Science* **2004**, *306*, 666. (b) Zhang, Y.; Tan, Y.-W.; Stormer, H. L.; Kim, P. *Nature* **2005**, *438*, 201.

CR068010R